

DIRAC ASSISTED TREE METHOD FOR 1D HETEROGENEOUS HELMHOLTZ EQUATIONS WITH ARBITRARY VARIABLE WAVE NUMBERS

BIN HAN, MICHELLE MICHELLE, AND YAU SHU WONG

ABSTRACT. One-dimensional Helmholtz equations have been well studied in the literature for moderately large wave numbers. In this paper we introduce a method called Dirac Assisted Tree (DAT), which can handle heterogeneous Helmholtz equations with arbitrarily large variable wave numbers. DAT breaks an original global problem into many parallel tree-structured small local problems, which can be effectively solved. All such local solutions are then linked together to form a global solution by solving small Dirac assisted linking problems with an inherent tree structure. DAT is embedded with the following attractive features: domain decomposition for reducing the problem size, tree structure and tridiagonal matrices for computational efficiency, and adaptivity for further improved performance. In order to solve the local problems in DAT, we shall propose a *compact* finite difference scheme with arbitrarily high accuracy order and low numerical dispersion for piecewise smooth coefficients and variable wave numbers. Such schemes are particularly appealing for DAT, because the local problems and their fluxes in DAT can be computed with high accuracy. With the aid of such high-order compact finite difference schemes, DAT can solve heterogeneous Helmholtz equations with arbitrarily large variable wave numbers accurately by solving small linear systems — 4×4 matrices in the extreme case — with tridiagonal coefficient matrices in a parallel fashion. Several examples will be provided to illustrate the effectiveness of DAT and compact finite difference schemes in numerically solving heterogeneous Helmholtz equations with variable wave numbers. We shall also discuss how to solve some special two-dimensional Helmholtz equations using DAT developed for one-dimensional problems. As demonstrated in all our numerical experiments, the convergence rates of DAT measured in relative L_2 , L_∞ and H^1 energy norms as a result of using our M -th order compact finite difference scheme are of order M . In all our numerical examples, we shall take $M = 6$ and $M = 8$.

1. INTRODUCTION AND MOTIVATIONS

The heterogeneous Helmholtz equation is given by

$$\nabla \cdot (a(x)\nabla u(x)) + \kappa^2(x)u(x) = f(x), \quad x \in \Omega \quad (1.1)$$

coupled with suitable boundary conditions on the boundary $\partial\Omega$ of the computational domain Ω , where the source term $f \in L_2(\Omega)$ and the coefficients $a, \kappa \in L_\infty(\Omega)$ satisfying $\text{ess-inf}_{x \in \Omega} a(x) > 0$. In this paper, we mainly focus on one-dimensional (1D) heterogeneous Helmholtz equation with $\Omega = (0, 1)$, and particular two-dimensional Helmholtz equations which can be converted and solved through 1D Helmholtz equations. To absorb outgoing waves, we shall use Sommerfeld absorbing boundary condition for one or both endpoints on $(0, 1)$. In practical applications, the coefficients a , the wave number κ and the source term f in (1.1) are often piecewise smooth functions.

The Helmholtz equation is known to be a challenging problem in computational mathematics due to the presence of the pollution effect caused by large wave numbers and the highly ill-conditioned coefficient matrix due to its discretization (e.g., see [7]). The former means that one cannot simply decrease the grid size in proportion to the growth in the wave number, but rather its reduction has to significantly outweigh the growth of the wave number to reduce the pollution effect (i.e., numerical dispersion). In the presence of a very large constant wave number, this means that standard Finite Element Method (FEM) and Finite Difference Method (FDM) inevitably yield a very large

2020 *Mathematics Subject Classification.* 65L12, 65N06, 35J05.

Key words and phrases. heterogeneous Helmholtz equation, variable wave number, accuracy order, numerical dispersion, compact finite difference method, Dirac distribution.

Corresponding author: Bin Han (bhan@ualberta.ca) at University of Alberta. Research supported in part by Natural Sciences and Engineering Research Council (NSERC) of Canada and Alberta Innovates.

ill-conditioned coefficient matrix. More specifically, the authors in [18] found that to properly handle a large constant wave number κ in the hp -FEM setting, the polynomial degree p and the mesh size h need to be chosen such that $p \gtrsim \log(\kappa)$ and the quantity $\kappa h/p$ is small enough. On the other hand, it has been documented that for second-order and fourth-order FDM, the appropriate resolution conditions are respectively $\kappa^3 h^2 \lesssim 1$ and $\kappa^5 h^4 \lesssim 1$ [5, 6, 27]. Generally speaking, for polynomial-based schemes like standard FEM and FDM, the higher the order a scheme has, the better it is in dealing with the pollution effect.

There is a vast array of methods developed over the years to deal with the demanding resolution condition on the mesh size h discussed above. In the Galerkin setting, one approach is to relax the inter-element continuity condition [8] or to impose a penalty on the normal jump of the derivatives of elements in trial and test spaces [3, 27]. Another way is to enrich the local approximation space with solutions of the homogeneous Helmholtz equation. This approach is commonly called Trefftz methods. See the survey article [14] and many references therein for more details.

In the FDM setting, numerous schemes with various accuracy, dispersion orders and stencil sizes can be found in the literature [2, 5, 6, 9–11, 20, 22–25, 30, 32]. Furthermore, a pollution-free finite difference scheme for 1D Helmholtz equation with a constant wave number in homogeneous media is available [27, 29, 31]. A wave splitting method for 1D Helmholtz equation was analyzed in [19]. Many preconditioners and domain decomposition methods have also been proposed for numerical solutions of Helmholtz equations. See the survey article [13] and references therein.

Most of the studies and papers cited above mainly deal with constant or smoothly varying wave numbers in homogeneous media. There are significantly fewer studies for the heterogeneous Helmholtz equation (e.g., [4, 12]). In the context of FDM, the authors in [2] provided a fourth-order compact finite difference scheme under the assumptions that the coefficient $a(x)$ and the wave number κ are smooth functions. The heterogeneous Helmholtz equation is indeed even harder to solve numerically, because we need to capture extra fine scale features on top of the oscillations introduced by the large wave number if the coefficient $a(x)$ in (1.1) is rough. Nevertheless, it is of particular interest to study such an equation, since it shows up in many applications like geophysics and ocean acoustics. More precisely, the heterogeneous Helmholtz equation models the way acoustic wave travels in a layered underground or underwater.

Our goal of this paper is to develop numerical schemes with high accuracy order for solving 1D heterogeneous Helmholtz equation *with arbitrarily large variable wave numbers, but without solving enormous ill-conditioned linear systems of equations*. To achieve our goal, we shall develop the Dirac Assisted Tree (DAT) method and compact finite difference schemes with arbitrarily high accuracy order. The key idea of DAT is to break the global problem on $[0, 1]$ into many small local problems which can be effectively solved by any known methods in a parallel fashion. Such local solutions are then stitched together into a desired global solution through solving many small linking problems in a parallel fashion as well. As a consequence, this leads to parallel systems of linear equations which have much smaller condition numbers and are significantly smaller in size.

More specifically, we multiply the source term f with a partition of unity on $[0, 1]$ to break the global source term f into many highly localized source terms f_j for $1 \leq j \leq N_0$ such that $\sum_{j=1}^{N_0} f_j = f$. For simplicity, we shall use hat linear functions (i.e., the B-spline of order 2) to create a partition of unity. Other choices like higher order B-splines or piecewise smooth functions are also permissible. Then for each highly localized source term f_j , we solve a local 1D Helmholtz equation on the subinterval of the support of f_j . With the exception of local problems that touch the boundaries 0 or 1, we impose homogeneous Dirichlet boundary conditions for all local problems. Such local problems can be solved by any known discretization method, provided that the fluxes at the endpoints of local problems can be accurately computed (see Section 2 for details). In order to assemble all the local solutions into a global solution, we shall see in Section 2 that the Dirac distribution will naturally appear in the fluxes of local solutions. Indeed using the Dirac distribution, we can naturally link all such local solutions together via DAT. Due to the refinability of the hat function, the local problems

can be further decomposed into sub-local problems. Applying this recursively, we obtain the tree structure of DAT. As we shall see in Section 2, DAT enjoys the following inherent advantages:

- (1) The accuracy of DAT only depends on the accuracy of the local problem solvers. Ideally, if all local problems can be solved without any error, then DAT yields the exact solution.
- (2) DAT breaks the global problem into tree-structured small local problems, which can be solved by any methods with reduced pollution effect. All such local solutions are then linked together to form a global solution by solving small linking problems.
- (3) All involved local and linking problems in DAT can be solved in a parallel manner by solving small linear systems often with significantly smaller condition numbers. Extremely speaking, all local and linking problems in DAT can be solved in a parallel manner by solving only at most 4 linear equations.
- (4) DAT naturally brings about domain decomposition, which reduces the problem size, and adaptivity, which further improves the approximation. It is efficient due to its tree structure and tridiagonal coefficient matrices.
- (5) Without imposing any magnitude constraints on variable wave numbers, DAT can solve heterogeneous Helmholtz equations with arbitrarily large variable wave numbers, which other known methods have difficulties in handling.

In order to solve the local problems in DAT and to reduce the numerical dispersion, for piecewise smooth coefficients and variable wave numbers, in this paper we shall propose a *compact* finite difference scheme with arbitrarily high accuracy order. As stated earlier, there is an abundance of finite difference schemes in the literature. Our second contribution is to rigorously prove that we can always find a 1D compact finite difference scheme (that handles both interior and any boundary conditions) with arbitrarily high accuracy orders by assuming that a, κ^2, f are piecewise smooth. In a much simpler setting with $a = 1$ and $\kappa^2 = 0$, [21, Theorem 3.1] already showed that we can always find an arbitrarily accurate compact finite difference scheme for the 1D Poisson equation with Dirichlet boundary conditions. Our result generalizes this statement. It also unifies many 1D finite difference schemes for the equations of the type (1.1) including $\kappa^2(x)$ in (1.1) being replaced by $-\kappa^2(x)$ (i.e., a standard elliptic problem). Compact stencils are very much desirable, since they give rise to a tridiagonal matrix in the 1D setting. Without losing any accuracy order, our approach can indeed handle all Dirichlet, Neumann, and Robin boundary conditions. Such high order compact finite difference schemes are particularly appealing for DAT, since the fluxes and derivatives of the local solutions can be computed accurately. This preserves the high accuracy of all our linking problems. As a consequence, in the presence of a very large wave number, we avoid dealing with a very large ill-conditioned coefficient matrix altogether. Instead, we harness parallel computing resources to solve small and much better conditioned coefficient matrices. This makes DAT a very attractive alternative when dealing with heterogeneous Helmholtz equations.

Next, we discuss how our method differs from the partition of unity FEM (PUFEM) presented in [1, 17]. Refer to Table 1 for a brief comparison of the numerical performance between DAT, 6-th and 8-th order FDM, as well as PUFEM (see [1, Section 3] for special shape functions used in 1D PUFEM and the corresponding coefficient matrix). One stark difference is in how we apply the partition of unity. Recall that DAT applies the partition of unity to the source term f . By the definition of PUFEM, we multiply the partition of unity with local approximation spaces and use this as our test and trial spaces in FEM. The effectiveness of PUFEM hinges on how to find suitable local approximation spaces. For the case of $a(x) = 1$ and a constant wave number, the local approximation spaces take the form of plane waves or generalized harmonic polynomials. In the presence of a large wave number, the trial functions in PUFEM are highly oscillatory. Hence, selecting/developing an appropriate quadrature becomes a major concern and challenge for PUFEM. Moreover, numerical experiments in [26] indicate that the coefficient matrix of PUFEM has an extremely large condition number, which may produce extra stability issues. For the heterogeneous Helmholtz equation with piecewise smooth coefficients and wave number, finding suitable local approximation spaces can in

fact be challenging and computationally expensive. See [12] for some work along this direction. We also note that DAT is not a variation of multigrid method either. Strictly speaking, DAT operates with one size grid. Due to the partition of unity, the local problems allow us to focus on different sub-domains, but with the same original grid size. This is why as we further decompose the local problems, our coefficient matrices continue to reduce in size.

Example 1. To illustrate the performance of DAT, we provide here one simple numerical example for the 1D Helmholtz equation:

$$u'' + \kappa^2 u = f \quad \text{on } [0, 1] \quad \text{with } u(0) = 0, \quad u'(1) - i\kappa u(1) = 0, \quad (1.2)$$

where $\kappa = 10^6$ and $f(x) = \kappa^2 \cosh(x)$. Note that the exact analytic solution u_e of (1.2) is

$$u_e = \frac{-\kappa \sin(\kappa x)}{\kappa^2 + 1} (\sinh(1) - i \cosh(1)\kappa) e^{i\kappa} + \frac{\kappa^2 (\cosh(x) - e^{i\kappa x})}{\kappa^2 + 1}.$$

See Table 1 for the relative errors of numerical solutions $u_N := \{u_N(j/N)\}_{j=0}^N$ obtained by DAT, FDM, and PUFEM, where both DAT (for solving local problems) and FDM use the same compact finite difference schemes with 6-th and 8-th accuracy order described in Subsection 3.4. Because the wave number $\kappa = 10^6$ is large, for fair comparison of our proposed DAT with PUFEM, all inner products in PUFEM are calculated exactly via symbolic computation to minimize possible errors due to numerical quadrature. All local and linking problems in DAT in Table 1 solve at most 4×4 linear systems. Table 1 demonstrates that DAT can handle very small mesh size and the maximum condition numbers of coefficient matrices coming from all local and linking problems are much smaller than those in FDM and PUFEM by several orders of magnitude.

N	$\frac{\ u_N - u_e\ _\infty}{\ u_e\ _\infty}$	$\frac{\ u'_N - u'_e\ _\infty}{\ u'_e\ _\infty}$	$\frac{\ u_N - u_e\ _2}{\ u_e\ _2}$	$\frac{\ u'_N - u'_e\ _2}{\ u'_e\ _2}$	$\frac{\ u_N - u_e\ }{\ u_e\ }$	Local CN	Link CN
DAT with 6-th order FDM described in Subsection 3.4							
2^{21}	1.7276×10^{-1}	4.0087×10^{-1}	1.6586×10^{-1}	2.8187×10^{-1}	2.0216×10^{-1}	3.2293×10^1	4.1813×10^2
2^{22}	2.6379×10^{-3}	6.1212×10^{-3}	2.6495×10^{-3}	4.5026×10^{-3}	3.2293×10^{-3}	4.1525×10^1	6.3689×10^1
2^{23}	4.0946×10^{-5}	9.5014×10^{-5}	4.1154×10^{-5}	6.9940×10^{-5}	5.0162×10^{-5}	4.4111×10^1	6.2854×10^1
FDM with 6-th order accuracy described in Subsection 3.4							
2^{21}	1.7276×10^{-1}	4.0087×10^{-1}	1.6586×10^{-1}	2.8187×10^{-1}	2.0216×10^{-1}	1.6050×10^7	—
2^{22}	2.6379×10^{-3}	6.1212×10^{-3}	2.6495×10^{-3}	4.5026×10^{-3}	3.2293×10^{-3}	7.1535×10^7	—
2^{23}	4.0945×10^{-5}	9.5012×10^{-5}	4.1154×10^{-5}	6.9938×10^{-5}	5.0160×10^{-5}	3.5067×10^8	—
DAT with 8-th order FDM described in Subsection 3.4							
2^{21}	4.3849×10^{-4}	1.0173×10^{-3}	4.4077×10^{-4}	7.4885×10^{-4}	5.3716×10^{-4}	3.2294×10^1	6.2702×10^1
2^{22}	1.6671×10^{-6}	3.8677×10^{-6}	1.6755×10^{-6}	2.8467×10^{-6}	2.0420×10^{-6}	4.1525×10^1	6.2841×10^1
2^{23}	1.1594×10^{-8}	2.6901×10^{-8}	1.1513×10^{-8}	1.9563×10^{-8}	1.4032×10^{-8}	4.4111×10^1	6.2841×10^1
FDM with 8-th order accuracy described in Subsection 3.4							
2^{21}	4.3849×10^{-4}	1.0173×10^{-3}	4.4077×10^{-4}	7.4885×10^{-4}	5.3716×10^{-4}	2.0738×10^7	—
2^{22}	1.6674×10^{-6}	3.8683×10^{-6}	1.6758×10^{-6}	2.8470×10^{-6}	2.0422×10^{-6}	8.6503×10^7	—
2^{23}	8.1795×10^{-9}	1.8977×10^{-8}	7.9889×10^{-9}	1.3574×10^{-8}	9.7363×10^{-9}	3.5067×10^8	—
PUFEM in [1]							
2^{21}	1.2806×10^{-1}	5.7930×10^{-1}	1.6595×10^{-1}	3.4629×10^{-1}	2.2649×10^{-1}	2.0807×10^7	—
2^{22}	3.2473×10^{-2}	2.1123×10^{-1}	4.2082×10^{-2}	1.2194×10^{-1}	7.1693×10^{-2}	8.6789×10^7	—
2^{23}	8.1473×10^{-3}	8.9740×10^{-2}	1.0558×10^{-2}	5.2347×10^{-2}	2.8064×10^{-2}	2.3750×10^8	—

TABLE 1. Relative errors (defined in (4.1) and (4.2)) using DAT, FDM, and PUFEM for solving Example 1. The grid increment used in $[0, 1]$ is N^{-1} . The tree levels in DAT are respectively 19, 20, and 21. “Local CN” and “Link CN” stand for the maximum condition numbers of coefficient matrices in all local and linking problems in DAT, respectively. “Local CN” for FDM and PUFEM just lists their corresponding condition numbers. The errors for PUFEM are evaluated at nodal points.

The organization of this paper is as follows. In Section 2, we present and discuss the Dirac Assisted Tree (DAT) method. In Section 3, to solve the local problems in DAT, we prove that we can always find a 1D compact finite difference scheme with arbitrarily high accuracy order for 1D Helmholtz equation in (1.1) with piecewise smooth coefficients, wave numbers, and source terms. A few examples

of such a scheme are also presented in this section. We show how the lower order schemes can be easily recovered from the higher order ones. Finally, we apply DAT by employing the finite difference schemes discussed in Section 3 as local problem solvers to some 1D and 2D problems, and then evaluate its numerical performance in Section 4.

2. DIRAC ASSISTED TREE (DAT) METHOD

In this section we shall discuss the key ingredients and algorithm for the Dirac Assisted Tree (DAT) method. The DAT method discussed in this section can be generalized to any general linear differential operator \mathcal{L} with appropriate modification. Let \mathcal{L} be the associated linear differential operator of the one-dimensional heterogeneous Helmholtz equations in (1.1) with $\Omega = (0, 1)$. More explicitly,

$$\mathcal{L}u := [a(x)u'(x)]' + \kappa^2(x)u(x) = f(x), \quad x \in \Omega := (0, 1) \quad (2.1)$$

with any given linear boundary conditions

$$\mathcal{B}_0 u(0) := \lambda_0^L u(0) + \lambda_1^L u'(0) = g_0, \quad \mathcal{B}_1 u(1) := \lambda_0^R u(1) + \lambda_1^R u'(1) = g_1, \quad (2.2)$$

where $\lambda_0^L, \lambda_1^L, \lambda_0^R, \lambda_1^R \in \mathbb{C}$ satisfying $|\lambda_0^L| + |\lambda_1^L| \neq 0$ and $|\lambda_0^R| + |\lambda_1^R| \neq 0$. I.e., $\mathcal{B}_0 u(0)$ and $\mathcal{B}_1 u(1)$ can be Dirichlet, Neumann or Robin (e.g. Sommerfeld) boundary conditions.

Let $(\alpha, \beta) \subseteq (0, 1)$ be a subinterval of Ω with $0 \leq \alpha < \beta \leq 1$. Let $f \in H^{-1}(\alpha, \beta)$ be a source term. Let $u_{loc} \in H^1(\alpha, \beta)$ be the weak solution to the following local problem:

$$\mathcal{L}u_{loc}(x) = f(x), \quad x \in (\alpha, \beta), \quad (2.3)$$

where the boundary conditions are given by $\mathcal{B}_0 u_{loc}(0) = g_0$ for $\alpha = 0$ (i.e., the same boundary condition as in (2.2) at 0), and $u_{loc}(\alpha) = 0$ for $\alpha > 0$ (i.e., homogeneous Dirichlet boundary condition at α), while $\mathcal{B}_1 u_{loc}(1) = g_1$ for $\beta = 1$ (i.e., the same boundary condition as in (2.2) at 1), and $u_{loc}(\beta) = 0$ for $\beta < 1$. In short, if $\alpha, \beta \in \{0, 1\}$, then we preserve the boundary conditions as in (2.2); otherwise, we use homogeneous Dirichlet boundary conditions. Putting these boundary conditions into a compact form, the boundary conditions to (2.3) are given by

$$(\mathcal{B}_0 u_{loc}(0) - g_0)\delta_{0,\alpha} + (1 - \delta_{0,\alpha})u_{loc}(\alpha) = 0, \quad (\mathcal{B}_1 u_{loc}(1) - g_1)\delta_{1,\beta} + (1 - \delta_{1,\beta})u_{loc}(\beta) = 0,$$

where $\delta_{c,c} = 1$ and $\delta_{c,d} = 0$ for $c \neq d$. Recall that $\psi \in H^1(\alpha, \beta)$ if $\psi \in L_2(\alpha, \beta)$ and its weak/distributional derivative $\psi' \in L_2(\alpha, \beta)$. Moreover, $\|\psi\|_{H^1(\alpha,\beta)}^2 := \|\psi\|_{L_2(\alpha,\beta)}^2 + \|\psi'\|_{L_2(\alpha,\beta)}^2$, where ψ' stands for the weak derivative of ψ . Obviously, due to our prescribed boundary conditions, we have $u_{loc} \in H^1(\alpha, \beta) \subseteq H^1(0, 1)$. Therefore, we can define a distribution

$$\tilde{f}(x) := \mathcal{L}u_{loc}(x), \quad x \in \Omega = (0, 1). \quad (2.4)$$

Now using the definition of the linear differentiation operator \mathcal{L} in (2.1), we conclude that

$$\tilde{f} = \begin{cases} 0, & x \in (0, \alpha), \\ d_\alpha(u_{loc})\delta_\alpha, & x = \alpha \text{ and } \alpha \neq 0, \\ f(x), & x \in (\alpha, \beta), \\ d_\beta(u_{loc})\delta_\beta, & x = \beta \text{ and } \beta \neq 1, \\ 0, & x \in (\beta, 1), \end{cases} \quad (2.5)$$

where δ_α is the Dirac distribution at the point α and the numbers $d_\alpha(u_{loc}), d_\beta(u_{loc}) \in \mathbb{C}$ for $\alpha \neq 0$ and $\beta \neq 1$ are given by

$$d_\alpha(u_{loc}) := \lim_{x \rightarrow \alpha^+} a(x)u'_{loc}(x), \quad d_\beta(u_{loc}) := - \lim_{x \rightarrow \beta^-} a(x)u'_{loc}(x), \quad (2.6)$$

which, up to a sign change, are simply the fluxes of u_{loc} at the endpoints α and β . Now extend $u_{loc} \in H^1(\alpha, \beta)$ as an element in $H^1(0, 1)$ by zero extension. Then it is easy to observe that u_{loc} is a global solution of

$$\mathcal{L}u_{loc}(x) = \tilde{f}(x), \quad x \in \Omega = (0, 1).$$

We now introduce the Dirac Assisted Tree (DAT) method. Let $N_0 \in \mathbb{N}$ be a positive integer greater than one. We take a partition of unity $\{\varphi_j\}_{j=0}^{N_0}$ of piecewise smooth functions such that each function φ_j is supported on $[0, 1]$ and $\sum_{j=0}^{N_0} \varphi_j(x) = 1$ for all $x \in (0, 1)$. For simplicity, we take piecewise linear hat functions φ_j as follows. Let $0 = x_0 < \dots < x_{N_0-1} < x_{N_0} = 1$ be a partition of the interval $[0, 1]$. For simplicity, we define $x_{-1} = 0$ and $x_{N_0+1} := 1$. We let φ_j be the linear hat function supported on $[x_{j-1}, x_{j+1}]$ with $\varphi_j(x_j) = 1$ and $\varphi_j(x_{j-1}) = \varphi_j(x_{j+1}) = 0$. Obviously, we define $\varphi_0(x_0) = 1$ and $\varphi_0(x_1) = 0$, while $\varphi_{N_0}(x_{N_0}) = 1$ and $\varphi_{N_0}(x_{N_0-1}) = 0$. We now partition the original source function f into small pieces as follows:

$$f_j(x) := f(x)\varphi_j(x), \quad j = 0, \dots, N_0.$$

Since $\sum_{j=0}^{N_0} \varphi_j(x) = 1$ for all $x \in (0, 1)$, we have $f = \sum_{j=0}^{N_0} f_j$. Let $u_j \in H^1(x_{j-1}, x_{j+1})$ be the weak solution to the local problem:

$$\mathcal{L}u_j(x) = f_j(x), \quad x \in (x_{j-1}, x_{j+1}) \quad (2.7)$$

with the boundary conditions:

$$\begin{aligned} (\mathcal{B}_0 u_j(0) - g_0 \delta_{0,j}) \delta_{0,x_{j-1}} + (1 - \delta_{0,x_{j-1}}) u_j(x_{j-1}) &= 0, \\ (\mathcal{B}_1 u_j(1) - g_1 \delta_{M,j}) \delta_{1,x_{j+1}} + (1 - \delta_{1,x_{j+1}}) u_j(x_{j+1}) &= 0. \end{aligned} \quad (2.8)$$

That is, we use the homogeneous Dirichlet boundary conditions $u_j(x_{j-1}) = u_j(x_{j+1}) = 0$, except $\mathcal{B}_0 u_0(0) = g_0$, $\mathcal{B}_0 u_1(0) = 0$, $\mathcal{B}_1 u_{N_0}(1) = g_1$, and $\mathcal{B}_1 u_{N_0-1}(1) = 0$. Since $u_j \in H^1(x_{j-1}, x_{j+1}) \subset H^1(0, 1)$, as we explained before, we must have

$$\tilde{f}_j(x) := \mathcal{L}u_j(x) = \begin{cases} 0, & x \in (0, x_{j-1}), \\ d_{x_{j-1}}(u_j) \delta_{x_{j-1}}, & x = x_{j-1} \text{ and } x_{j-1} \neq 0, \\ f_j(x), & x \in (x_{j-1}, x_{j+1}), \\ d_{x_{j+1}}(u_j) \delta_{x_{j+1}}, & x = x_{j+1} \text{ and } x_{j+1} \neq 1, \\ 0, & x \in (x_{j+1}, 1). \end{cases} \quad (2.9)$$

Now we discuss how to link/stitch all these local solutions $\{u_j\}_{j=0}^{N_0}$ together. To do so, for $j = 1, \dots, N_0 - 1$, we solve the following Dirac-assisted local problem:

$$\mathcal{L}v_j(x) = \delta_{x_j}, \quad x \in (x_{j-1}, x_{j+1}) \quad (2.10)$$

with the boundary conditions:

$$\begin{aligned} \mathcal{B}_0 v_j(0) \delta_{0,x_{j-1}} + (1 - \delta_{0,x_{j-1}}) v_j(x_{j-1}) &= 0, \\ \mathcal{B}_1 v_j(1) \delta_{1,x_{j+1}} + (1 - \delta_{1,x_{j+1}}) v_j(x_{j+1}) &= 0. \end{aligned} \quad (2.11)$$

That is, we use the homogeneous Dirichlet boundary condition $v_j(x_{j-1}) = v_j(x_{j+1}) = 0$, except $\mathcal{B}_0 v_1(0) = 0$ and $\mathcal{B}_1 v_{N_0-1}(1) = 0$. Since $v_j \in H^1(x_{j-1}, x_{j+1}) \subset H^1(0, 1)$, as we explained before, we must have

$$\tilde{\delta}_{x_j}(x) := \mathcal{L}v_j(x) = \begin{cases} 0, & x \in (0, x_{j-1}), \\ d_{x_{j-1}}(v_j) \delta_{x_{j-1}}, & x = x_{j-1} \text{ and } x_{j-1} \neq 0, \\ \delta_{x_j}, & x \in (x_{j-1}, x_{j+1}), \\ d_{x_{j+1}}(v_j) \delta_{x_{j+1}}, & x = x_{j+1} \text{ and } x_{j+1} \neq 1, \\ 0, & x \in (x_{j+1}, 1). \end{cases} \quad (2.12)$$

To link all the local solutions $\{u_j\}_{j=0}^{N_0}$ together, we need the following result.

Theorem 2.1. *The elements in $\{v_1, \dots, v_{N_0-1}\}$ are linearly independent and for any complex numbers $\mu_j, j = 1, \dots, N_0 - 1$, the following linear system induced by*

$$\sum_{j=1}^{N_0-1} \tilde{\mu}_j \tilde{\delta}_{x_j} = \sum_{j=1}^{N_0-1} \mu_j \delta_{x_j} \quad (2.13)$$

has a unique solution $\{\tilde{\mu}_j\}_{j=1}^{N_0-1}$. Moreover, $V = W$, where V is the linear span of $\{v_j\}_{j=1}^{N_0-1}$ and W is the linear span of $\{w_j\}_{j=1}^{N_0-1}$, where w_j is the weak solution to

$$\mathcal{L}w_j(x) = \delta_{x_j}, \quad x \in (0, 1) \quad \text{with} \quad \mathcal{B}_0w_j(0) = 0, \quad \mathcal{B}_1w_j(1) = 0. \quad (2.14)$$

Proof. Since $\mathcal{L}v_j = \tilde{\delta}_{x_j}$ on $(0, 1)$ and $v_j(0) = v_j(1) = 0$ except $\mathcal{B}_0v_1(0) = 0$ and $\mathcal{B}_1v_{N_0-1}(1) = 0$, we obviously have $v_j \in W$ and hence $V \subseteq W$. We now prove that the elements in $\{v_1, \dots, v_{N_0-1}\}$ are linearly independent. To do so, we claim that it is impossible that either $v_j|_{(x_{j-1}, x_j)}$ or $v_j|_{(x_j, x_{j+1})}$ can be identically zero. Without loss of generality, we assume that $v_j|_{(x_{j-1}, x_j)}$ is identically zero. Since $v_j \in H^1(x_{j-1}, x_{j+1})$, the function v_j is continuous on (x_{j-1}, x_{j+1}) and hence $v_j(x_j) = 0$. However, since v_j is the weak solution to the local linking problem in (2.10), we see that $\tilde{v}_j := v_j|_{(x_j, x_{j+1})}$ must be the weak solution to $\mathcal{L}\tilde{v}_j(x) = 0$ on (x_j, x_{j+1}) with the boundary conditions $\tilde{v}_j(x_j) = 0$ and $\tilde{v}_j(x_{j+1}) = 0$ (if $j = N_0 - 1$, then $x_{j+1} = 1$ and replace $\tilde{v}_j(x_{j+1}) = 0$ by $\mathcal{B}_1\tilde{v}_{N_0-1}(1) = 0$). By the uniqueness of the solution, the weak solution \tilde{v}_j must be identically zero. Hence, v_j must be identically zero, which contradicts (2.10). Hence, both $v_j|_{(x_{j-1}, x_j)}$ and $v_j|_{(x_j, x_{j+1})}$ cannot be identically zero.

Consider the linear combination $v := \sum_{j=1}^{N_0-1} \mu_j v_j$ such that v is identically zero. Because v_j is supported inside (x_{j-1}, x_{j+1}) , we have $0 = v|_{(x_0, x_1)} = \mu_1 v_1|_{(x_0, x_1)}$. Since $v_1|_{(x_0, x_1)}$ cannot be identically zero, we must have $\mu_1 = 0$. By induction on j , we must have $\mu_1 = \mu_2 = \dots = \mu_{N_0-1} = 0$. This proves that the elements in $\{v_j\}_{j=1}^{N_0-1}$ must be linearly independent. Now by $V \subseteq W$, we conclude that $V = W$. The uniqueness of the solution to the linear system in (2.13) follows straightforwardly, since $\mathcal{L}v_j = \tilde{\delta}_{x_j}$, $\mathcal{L}w_j = \delta_{x_j}$ and $V = W$. \square

The following result is the main ingredient of our Dirac Assisted Tree (DAT) method.

Theorem 2.2. *Define*

$$u := u_f + u_\delta \quad \text{with} \quad u_f := \sum_{j=0}^{N_0} u_j, \quad u_\delta := \sum_{j=1}^{N_0-1} \mu_j v_j, \quad (2.15)$$

where u_j is the weak solution to (2.7) with prescribed boundary conditions in (2.8), v_j is the weak solution to (2.10) with the prescribed boundary conditions in (2.11), and $\{\mu_j\}_{j=1}^{N_0-1}$ is the unique solution to the following linear system for the linking problem:

$$\sum_{j=1}^{N_0-1} \mu_j \tilde{\delta}_{x_j} = - \sum_{j=1}^{N_0} (d_{x_j}(u_{j-1}) + d_{x_j}(u_{j+1})) \delta_{x_j}, \quad (2.16)$$

Then u must be the weak solution to the heterogeneous Helmholtz equation in (2.1) with the boundary conditions in (2.2).

Proof. Since $\sum_{j=0}^{N_0} f_j = f$, we can write

$$f(x) = \sum_{j=0}^{N_0} f_j(x) = \sum_{j=0}^{N_0} \tilde{f}_j(x) - \sum_{j=1}^{N_0-1} (d_{x_j}(u_{j-1}) + d_{x_j}(u_{j+1})) \delta_{x_j}. \quad (2.17)$$

By Theorem 2.1, there is a unique solution $\{\mu_j\}_{j=1}^{N_0-1}$ to (2.16). That is, the linking problem in (2.16) can be uniquely solved. Hence, using (2.17), we can further write

$$f(x) = \sum_{j=0}^{N_0} \tilde{f}_j(x) + \sum_{j=1}^{N_0-1} \mu_j \tilde{\delta}_{x_j}. \quad (2.18)$$

By the definition of u_j , we observe that

$$\mathcal{L}u_f(x) = \sum_{j=0}^{N_0} \tilde{f}_j(x), \quad x \in (0, 1)$$

with the boundary conditions $\mathcal{B}_0 u_f(0) = g_0$ and $\mathcal{B}_1 u_f(1) = g_1$.

On the other hand, by the definition of $\tilde{\delta}_{x_j}$, we have

$$\mathcal{L}u_\delta(x) = \sum_{j=1}^{N_0-1} \mu_j \tilde{\delta}_{x_j}, \quad x \in (0, 1)$$

and u_δ satisfies the boundary conditions $\mathcal{B}_0 u_\delta(0) = 0$ and $\mathcal{B}_1 u_\delta(1) = 0$. Thus, by (2.18) we have

$$\mathcal{L}u = \mathcal{L}u_f + \mathcal{L}u_\delta = \sum_{j=0}^{N_0} \tilde{f}_j(x) + \sum_{j=1}^{N_0-1} \mu_j \tilde{\delta}_{x_j} = f(x), \quad x \in (0, 1)$$

and u satisfies the prescribed boundary conditions in (2.2). \square

Obviously, we can recursively apply the above procedure to solve each of the local problems in (2.7) with prescribed boundary conditions in (2.8) to further reduce the size of the problem. To elucidate this point, we now present the Dirac Assisted Tree (DAT) algorithm below.

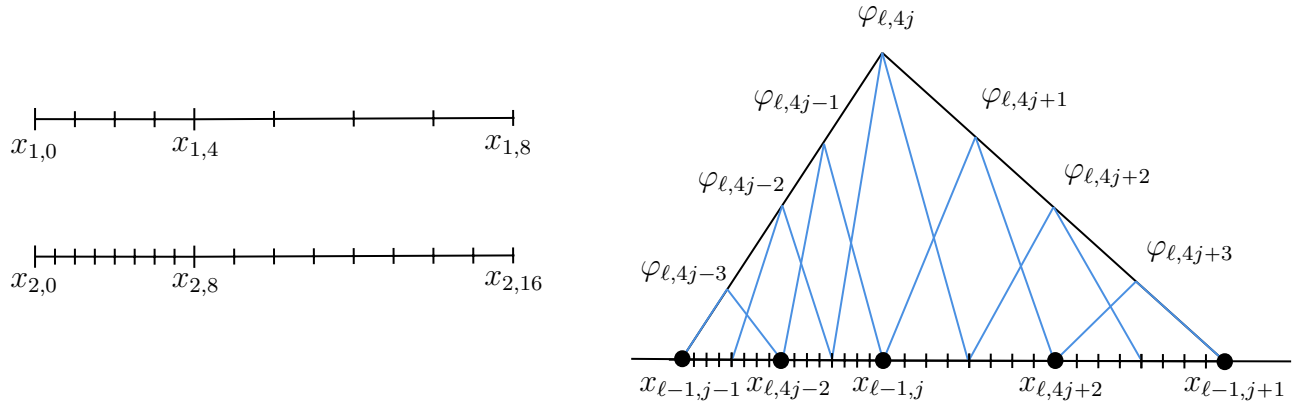


FIGURE 1. Left: An initial partition of $[0, 1]$ at $\ell = 1$ with $N_0 = 8$ and its subsequent refinement at $\ell = 2$ with $s = 1$. Right: The relationship between an interior large hat function $\varphi_{\ell-1,j}$ on $[x_{\ell-1,j-1}, x_{\ell-1,j+1}]$ and smaller hat functions $\varphi_{\ell,2^s j+k}$, $-2^s + 1 \leq k \leq 2^s - 1$, with $s = 2$.

Algorithm 1. Consider the 1-level partition $\{x_{1,j}\}_{j=0}^{N_0}$ given by $0 = x_{1,-1} = x_{1,0} < x_{1,1} < \dots < x_{1,N_0-1} < x_{1,N_0} = x_{1,N_0+1} = 1$, and let $\{\varphi_{1,j}\}_{j=0}^{N_0}$ be the associated partition of unity such that $\text{supp}(\varphi_{1,j}) \subseteq [x_{1,j-1}, x_{1,j+1}]$ with $\varphi_{1,j}(x_{1,j}) = 1$. Pick $L, s \in \mathbb{N}$ such that L is the tree level and any subinterval at a level is divided equally into 2^s small subintervals at the next level. For each tree level $\ell = 2, \dots, L$, let $\{x_{\ell,k}\}_{k=0}^{2^{\ell s} N_0}$ be a refinement partition of the grid $\{x_{\ell-1,k}\}_{k=0}^{2^{(\ell-1)s} N_0}$ such that $\{x_{\ell-1,k}\}_{k=0}^{2^{(\ell-1)s} N_0} \subset \{x_{\ell,k}\}_{k=0}^{2^{\ell s} N_0}$ with

$$x_{\ell-1,k} = x_{\ell,2^s k}, \quad x_{\ell,-1} := x_{\ell,0} = 0, \quad \text{and} \quad x_{\ell,2^{\ell s} N_0+1} := x_{\ell,2^{\ell s} N_0} = 1.$$

Fix a fine grid $\{x_j\}_{j=0}^N$, where $\{x_{L,k}\}_{k=0}^{N_0} \subset \{x_j\}_{j=0}^N$, on which the local problems will be solved. Note that $\text{supp}(\varphi_{\ell,j}) \subseteq [x_{\ell,j-1}, x_{\ell,j+1}]$ with $\varphi_{\ell,j}(x_{\ell,j}) = 1$ for $0 \leq j \leq 2^{(\ell-1)s} N_0$ and

$$\begin{aligned} \varphi_{\ell-1,0} &= \sum_{k=0}^{2^s-1} \varphi_{\ell,k}, & \varphi_{\ell-1,j} &= \sum_{k=-2^s+1}^{2^s-1} \varphi_{\ell,2^s j+k}, \quad j = 1, \dots, 2^{(\ell-2)s} N_0 - 1, \\ \varphi_{\ell-1,2^{(\ell-2)s} N_0} &= \sum_{k=-2^s+1}^0 \varphi_{\ell,2^{(\ell-1)s} N_0+k}. \end{aligned}$$

See Figure 1 for an illustration of the setting above.

- (S1) Solve the following local problems at tree level L in a parallel fashion using any chosen discretization method.

$$\begin{cases} \mathcal{L}u_{L,j} = f_j =: f\varphi_{L,j}, & x \in [x_{L,j-1}, x_{L,j+1}], & j = 0, \dots, 2^{(L-1)s}N_0 \\ (\mathcal{B}_0u_{L,j}(0) - g_0\delta_0(j))\delta_0(x_{L,j-1}) + (1 - \delta_0(x_{L,j-1}))u_{L,j}(x_{L,j-1}) = 0, \\ (\mathcal{B}_1u_{L,j}(1) - g_1\delta_{2^{L-1}N_0}(j))\delta_1(x_{L,j+1}) + (1 - \delta_1(x_{L,j+1}))u_{L,j}(x_{L,j+1}) = 0, \end{cases} \quad (2.19)$$

$$\begin{cases} \mathcal{L}v_{L,j} = \delta_{x_{L,j}}, & x \in [x_{L,j-1}, x_{L,j+1}], & j = 1, \dots, 2^{(L-1)s}N_0 - 1 \\ \mathcal{B}_0v_{L,j}(0)\delta_0(x_{L,j-1}) + (1 - \delta_0(x_{L,j-1}))v_{L,j}(x_{L,j-1}) = 0, \\ \mathcal{B}_1v_{L,j}(1)\delta_1(x_{L,j+1}) + (1 - \delta_1(x_{L,j+1}))v_{L,j}(x_{L,j+1}) = 0. \end{cases} \quad (2.20)$$

- (S2) Let $\ell = L, \dots, 2$ decreasingly. First, consider the net contribution of the artificial Dirac distributions at each grid point and find the appropriate linear combination of Dirac local problems to offset it. This allows us to recover the solutions to local problems at level $\ell - 1$ from those at level ℓ . More explicitly, solve the following linking problems in a parallel fashion for each ℓ .

- (a) (Left-most element of partition of unity)

Let $Q_{\ell,0}$ be a $(2^s - 1) \times (2^s - 1)$ tridiagonal matrix and $\gamma_{\ell,0}$ be a $(2^s - 1)$ vector with the following entries

$$(Q_{\ell,0})_{mn} = \begin{cases} d_{x_{\ell,m}}(v_{\ell,m+1}), & m < n, \\ 1, & m = n, \\ d_{x_{\ell,m}}(v_{\ell,m-1}), & m > n, \end{cases}$$

$$(\gamma_{\ell,0})_m = -d_{x_{\ell,m}}(u_{\ell,m-1}) - d_{x_{\ell,m}}(u_{\ell,m+1})(1 - \delta_{2^s-1}(m)),$$

where $m, n = 1, \dots, 2^s - 1$.

- (b) (Interior elements of partition of unity)

For all $j = 1, \dots, 2^{(\ell-2)s}N_0 - 1$, let $Q_{\ell,j}$ be a $(2^{s+1} - 1) \times (2^{s+1} - 1)$ tridiagonal matrix and $\gamma_{\ell,j}$ be a $(2^{s+1} - 1)$ vector with the following entries

$$(Q_{\ell,j})_{mn} = \begin{cases} d_{x_{\ell,2^s(j-1)+m}}(v_{\ell,2^s(j-1)+m+1}), & m < n, \\ 1, & m = n, \\ d_{x_{\ell,2^s(j-1)+m}}(v_{\ell,2^s(j-1)+m-1}), & m > n, \end{cases}$$

$$(\gamma_{\ell,j})_m = -d_{x_{\ell,2^s(j-1)+m}}(u_{\ell,2^s(j-1)+m-1})(1 - \delta_1(m))$$

$$- d_{x_{\ell,2^s(j-1)+m}}(u_{\ell,2^s(j-1)+m+1})(1 - \delta_{2^{s+1}-1}(m)),$$

where $m, n = 1, \dots, 2^{s+1} - 1$.

- (c) (Right-most element of partition of unity)

Let $Q_{\ell,2^{(\ell-2)s}N_0}$ be a $(2^s - 1) \times (2^s - 1)$ tridiagonal matrix and $\gamma_{\ell,2^{(\ell-2)s}N_0}$ be a $(2^s - 1)$ vector with the following entries

$$(Q_{\ell,2^{(\ell-2)s}N_0})_{mn} = \begin{cases} d_{x_{\ell,2^{(\ell-1)s}N_0-2^s+m}}(v_{\ell,2^{(\ell-1)s}N_0-2^s+m+1}), & m < n, \\ 1, & m = n, \\ d_{x_{\ell,2^{(\ell-1)s}N_0-2^s+m}}(v_{\ell,2^{(\ell-1)s}N_0-2^s+m-1}), & m > n, \end{cases}$$

$$(\gamma_{\ell,2^{(\ell-2)s}N_0})_m = -d_{x_{\ell,2^{(\ell-1)s}N_0-2^s+m}}(u_{\ell,2^{(\ell-1)s}N_0-2^s+m-1})(1 - \delta_1(m))$$

$$- d_{x_{\ell,2^{(\ell-1)s}N_0-2^s+m}}(u_{\ell,2^{(\ell-1)s}N_0-2^s+m+1}),$$

where $m, n = 1, \dots, 2^s - 1$.

- (d) (Construct the solutions to local problems at level $\ell - 1$)

Solve the linking problems $\mu_{\ell,j} = (Q_{\ell,j})^{-1}\gamma_{\ell,j}$ and $\nu_{\ell,j} = (Q_{\ell,j})^{-1}e_{2^s}$, where e_{2^s} is a

$(2^{s+1} - 1)$ vector with 1 in the 2^s -th entry and 0 in the remaining entries. Set

$$\begin{aligned} u_{\ell-1,0} &= \sum_{k=0}^{2^s-1} u_{\ell,k} + \sum_{k=1}^{2^s-1} (\mu_{\ell,0})_k v_{\ell,k}, \\ u_{\ell-1,j} &= \sum_{k=-2^s+1}^{2^s-1} u_{\ell,2^s j+k} + \sum_{k=1}^{2^{s+1}-1} (\mu_{\ell,j})_k v_{\ell,2^s j-2^s+k}, \\ v_{\ell-1,j} &= \sum_{k=1}^{2^{s+1}-1} (\nu_{\ell,j})_k v_{\ell,2^s j-2^s+k}, \\ u_{\ell-1,2^{(\ell-2)s}N_0} &= \sum_{k=-2^s+1}^0 u_{\ell,2^{(\ell-1)s}N_0+k} + \sum_{k=1}^{2^s-1} (\mu_{\ell,2^{(\ell-2)s}N_0})_k v_{\ell,2^{(\ell-1)s}N_0-2^s+k}. \end{aligned} \quad j = 1, \dots, 2^{(\ell-2)s}N_0 - 1,$$

(S3) Finally, the approximated solution of the problem (2.1)-(2.2) is given by

$$u = \sum_{k=0}^{N_0} u_{1,k} + \sum_{k=1}^{N_0-1} (\mu_{1,0})_k v_{0,k},$$

where $\mu_{1,0} = (Q_{1,0})^{-1}\gamma_{1,0}$, $Q_{1,0}$ is an $(N_0 - 1) \times (N_0 - 1)$ tridiagonal matrix with the following entries and $\gamma_{1,0}$ be an $(N_0 - 1)$ vector with the following entries

$$(Q_{1,0})_{mn} = \begin{cases} d_{x_{1,m}}(v_{1,m+1}), & m < n, \\ 1, & m = n, \\ d_{x_{1,m}}(v_{1,m-1}), & m > n, \end{cases}$$

$$(\gamma_{1,0})_m = -d_{x_{1,m}}(u_{1,m-1})(1 - \delta_1(m)) - d_{x_{1,m}}(u_{1,m+1})(1 - \delta_{N_0}(m)),$$

where $m, n = 1, \dots, N_0 - 1$.

As an illustrative example, if we take an equispaced grid on $[0, 1]$, $N_0 = 4$, $h = 2^{-n}$, $L = n - 2$, and $s = 1$, then each element of our partition of unity at this level (with the exception of the two boundaries) is supported on $[(j-1)2^{-n}, (j+1)2^{-n}]$ for $j = 1, \dots, 2^n - 1$. Consequently, each interior local problem in (S1) of Algorithm 1 that does not touch the boundary forms a 3×3 coefficient matrix. The matrix size becomes 4×4 if it touches the boundary point 0 or 1 whose original boundary condition is non-Dirichlet. The linking problem in (2.16) can be obtained by solving a 3×3 matrix equation. This exactly describes the situation in Examples 1 and 4.

3. COMPACT FINITE DIFFERENCE SCHEMES WITH ARBITRARILY HIGH ACCURACY ORDERS

To numerically solve the heterogeneous Helmholtz equation in (2.1)–(2.2) with piecewise smooth coefficients a, κ^2 and source term f , in this section we shall study compact finite difference schemes with arbitrarily high accuracy and numerical dispersion orders. Such compact finite difference schemes are of particular interest for accurately solving local problems stemming from DAT in the foregoing section.

3.1. Compact stencils for interior points. We start by stating a simple observation, which is critical for proving the existence of a 1D finite difference scheme with arbitrarily high accuracy order.

Proposition 3.1. *Let a, κ^2, f in (2.1) be smooth functions and let u be a smooth function satisfying $[a(x)u'(x)]' + \kappa^2(x)u(x) = f(x)$ for $x \in (0, 1)$. For any given point $x_b \in (0, 1)$, we have*

$$u^{(j)}(x_b) = E_{j,0}u(x_b) + E_{j,1}u'(x_b) + \sum_{\ell=0}^{j-2} F_{j,\ell}f^{(\ell)}(x_b), \quad j \geq 2, \quad (3.1)$$

where the quantities $E_{j,0}, E_{j,1}, F_{j,\ell}$ only depend on the values $a(x_b), a'(x_b), \dots, a^{(j-1)}(x_b)$ and $\kappa^2(x_b), [\kappa^2]'(x_b), \dots, [\kappa^2]^{(j-2)}(x_b)$ for $j \geq 2$ and $\ell \in \mathbb{N}_0$. Consequently, for sufficiently small h ,

$$u(x_b + h) = u(x_b)E_0(h) + u'(x_b)hE_1(h) + \sum_{\ell=0}^{\infty} h^{\ell+2} f^{(\ell)}(x_b)F_{\ell}(h), \quad (3.2)$$

where $E_0(h), E_1(h)$ and $F_{\ell}, \ell \in \mathbb{N}_0$ are defined to be

$$E_0(h) := 1 + \sum_{j=2}^{\infty} \frac{E_{j,0}}{j!} h^j, \quad E_1(h) := 1 + \sum_{j=2}^{\infty} \frac{E_{j,1}}{j!} h^{j-1}, \quad F_{\ell}(h) := \sum_{j=\ell+2}^{\infty} \frac{F_{j,\ell}}{j!} h^{j-\ell-2}. \quad (3.3)$$

Proof. We prove the claim in (3.1) using mathematical induction on j . Consider the base case with $j = 2$. Since $a(x) > 0$, we deduce from $[a(x)u'(x)]' + \kappa^2(x)u(x) = f(x)$ that

$$u^{(2)}(x) = -\frac{\kappa^2(x)}{a(x)}u(x) - \frac{a'(x)}{a(x)}u'(x) + \frac{f(x)}{a(x)}, \quad x \in (0, 1). \quad (3.4)$$

Hence, setting $x = x_b$ in the above identity (3.4), we conclude that (3.1) holds for $j = 2$.

Suppose that the claim in (3.1) holds for some $j \geq 2$. We now prove that (3.1) must hold for $j + 1$. Applying the $(j - 1)$ -th derivative to both sides of the identity in (3.4), we observe that

$$u^{(j+1)}(x) = -\left[\frac{\kappa^2(x)}{a(x)}u(x)\right]^{(j-1)} - \left[\frac{a'(x)}{a(x)}u'(x)\right]^{(j-1)} + \left[\frac{f(x)}{a(x)}\right]^{(j-1)}.$$

Applying the Leibniz differentiation formula to the above identity, we conclude that the quantity $u^{(j+1)}(x)$ can be written as a linear combination of $f(x), f'(x), \dots, f^{(j-1)}(x)$ and $u(x), u'(x), \dots, u^{(j)}(x)$ with all combination coefficients being smooth functions of x depending only on $a(x), a'(x), \dots, a^{(j)}(x)$ and $\kappa^2(x), [\kappa^2(x)]', \dots, [\kappa^2(x)]^{(j-1)}$. Now by induction hypothesis, we conclude that (3.1) holds for $j + 1$. This proves (3.1) by mathematical induction on j .

On the other hand, since u is smooth in a neighborhood of x_b , the Taylor series of u at the base point x_b is $u(x_b + h) = u(x_b) + u'(x_b)h + \sum_{j=2}^{\infty} \frac{u^{(j)}(x_b)}{j!} h^j$. Therefore, we deduce from (3.1) that

$$\begin{aligned} u(x_b + h) &= u(x_b) + u'(x_b)h + \sum_{j=2}^{\infty} \frac{h^j}{j!} \left(E_{j,0}u(x_b) + E_{j,1}u'(x_b) + \sum_{\ell=0}^{j-2} F_{j,\ell}f^{(\ell)}(x_b) \right) \\ &= u(x_b) \left(1 + \sum_{j=2}^{\infty} \frac{E_{j,0}}{j!} h^j \right) + u'(x_b) \left(h + \sum_{j=2}^{\infty} \frac{E_{j,1}}{j!} h^j \right) + \sum_{j=2}^{\infty} \sum_{\ell=0}^{j-2} \frac{F_{j,\ell}}{j!} h^j f^{(\ell)}(x_b) \\ &= u(x_b)E_0(h) + u'(x_b)hE_1(h) + \sum_{\ell=0}^{\infty} \sum_{j=\ell+2}^{\infty} \frac{F_{j,\ell}}{j!} h^j f^{(\ell)}(x_b), \end{aligned}$$

from which we obtain (3.2). \square

Using (3.4) and taking derivative on both sides of (3.1), we observe that the coefficients of $E_{j,0}, E_{j,1}$ and $F_{j,\ell}, \ell = 0, \dots, j - 2$ in Proposition 3.1 can be recursively obtained by

$$E_{j+1,0} = E'_{j,0} - \frac{\kappa^2}{a}E_{j,1}, \quad E_{j+1,1} = E_{j,0} + E'_{j,1} - \frac{a'}{a}E_{j,1}, \quad F_{j+1,\ell} = F'_{j,\ell} + F_{j,\ell-1}, \quad j \geq 2, \quad \ell = 0, \dots, j-1$$

with the initial values $E_{2,0} := -\frac{\kappa^2}{a}$ and $E_{2,1} := -\frac{a'}{a}$, and $F_{2,0} := \frac{1}{a}$, where we used the convention that $F_{j,-1} := \frac{E_{j,1}}{a}$ and $F_{j,\ell} := 0$ for all $\ell > j - 2$. Note that $E_0(0) = E_1(0) = 1$ and $F_{\ell}(0) = F_{\ell+2,\ell} = F_{2,0} = \frac{1}{a(x_b)}$ for all $\ell \in \mathbb{N}_0$.

Let us now consider compact finite difference schemes with high accuracy and numerical dispersion orders for the heterogeneous Helmholtz equation in (2.1) with smooth coefficients a, κ^2 and source term f . Suppose the discretization stencil is centered at an interior point x_b with mesh size $0 < h < 1$. That is, we fix the base point x_b to be in $(0, 1)$ such that $(x_b - h, x_b + h) \subset (0, 1)$.

Theorem 3.2. *Suppose that a, κ^2, f in (2.1) are smooth functions. Let M, \tilde{M} be positive integers with $M \geq \tilde{M}$. Let $0 < h < 1$ and $x_b \in (0, 1)$ such that $(x_b - h, x_b + h) \subset (0, 1)$. Consider the discretization stencil of a compact finite difference scheme for $\mathcal{L}u := [a(x)u'(x)]' + \kappa^2(x)u(x) = f(x)$ (i.e., (2.1)) at the base point x_b below*

$$\mathcal{L}_h u(x_b) := h^{-2}[c_{-1}(h)u(x_b - h) + c_0(h)u(x_b) + c_1(h)u(x_b + h)] - \sum_{\ell=0}^{\tilde{M}-1} d_\ell(h)h^\ell f^{(\ell)}(x_b), \quad (3.5)$$

where c_{-1}, c_0, c_1 and d_ℓ are smooth functions of h for $\ell = 0, \dots, \tilde{M} - 1$. Suppose that

$$\begin{aligned} c_1(h) &= \frac{\alpha(h)}{E_1(h)} + \mathcal{O}(h^{M+1}), & c_{-1}(h) &= \frac{\alpha(h)}{E_1(-h)} + \mathcal{O}(h^{M+1}), \\ c_0(h) &= -c_1(h)E_0(h) - c_{-1}(h)E_0(-h) + \mathcal{O}(h^{M+2}) \end{aligned} \quad (3.6)$$

and

$$d_\ell(h) = -\delta_{0,\ell} + c_1(h)F_\ell(h) + (-1)^\ell c_{-1}(h)F_\ell(-h) + \mathcal{O}(h^{\tilde{M}-\ell}), \quad \ell = 0, \dots, \tilde{M} - 1, \quad (3.7)$$

as $h \rightarrow 0$, where α is a smooth function of h with $\alpha(0) \neq 0$ and $E_0(h), E_1(h)$ and $F_\ell(h), \ell \in \mathbb{N}_0$ are defined uniquely in (3.3) of Proposition 3.1. Then the discretization stencil of the compact finite difference scheme has numerical dispersion order M at the base point x_b , that is,

$$h^{-2}[c_{-1}(h)u(x_b - h) + c_0(h)u(x_b) + c_1(h)u(x_b + h)] = \mathcal{O}(h^M), \quad h \rightarrow 0, \quad (3.8)$$

for every solution u of $\mathcal{L}u = 0$, and has accuracy order \tilde{M} at the base point x_b , that is,

$$\mathcal{L}_h u(x_b) - f(x_b) = \mathcal{O}(h^{\tilde{M}}), \quad h \rightarrow 0, \quad (3.9)$$

for every solution u of $\mathcal{L}u = f$.

Proof. By Proposition 3.1 and (3.1), all the quantities $E_{j,0}, E_{j,1}, F_{j,\ell}$ depend only on the values $a(x_b), a'(x_b), \dots, a^{(j-1)}(x_b)$ and $\kappa^2(x_b), [\kappa^2]'(x_b), \dots, [\kappa^2]^{(j-2)}(x_b)$ for $j \geq 2$ and $\ell \in \mathbb{N}_0$. For simplicity, we define $u_0 := u(x_b), u_1 := u'(x_b)$ and $f_\ell := f^{(\ell)}(x_b)$ for $\ell \in \mathbb{N}_0$. Therefore, by (3.2), we deduce that

$$\begin{aligned} h^2 \mathcal{L}_h u(x_b) - h^2 f_0 &= u_0 \left(c_{-1}(h)E_0(-h) + c_0(h) + c_1(h)E_0(h) \right) + u_1 h \left(-c_{-1}(h)E_1(-h) + c_1(h)E_1(h) \right) \\ &+ \sum_{\ell=0}^{\infty} h^{\ell+2} f_\ell \left(c_1(h)F_\ell(h) + (-1)^\ell c_{-1}(h)F_\ell(-h) \right) - (d_0(h) + 1)h^2 f_0 - \sum_{\ell=1}^{\tilde{M}-1} d_\ell(h)h^{\ell+2} f_\ell, \end{aligned} \quad (3.10)$$

where $E_0(h)$ and $E_1(h)$ are defined in (3.3).

On the other hand, from $f(x) = [a(x)u'(x)]' + \kappa^2(x)u(x)$ we trivially observe that $f^{(\ell)}$ can be written as a linear combination of $u, u', \dots, u^{(\ell+2)}$ as well. Consequently, (3.8) holds (or equivalently, (3.9) holds with $f = 0$ and $\tilde{M} = M$) for numerical dispersion order M if and only if the coefficients of u_0 and u_1 in the above identity are $\mathcal{O}(h^{M+2})$ as $h \rightarrow 0$. That is, (3.8) is equivalent to

$$\begin{aligned} c_{-1}(h)E_0(-h) + c_0(h) + c_1(h)E_0(h) &= \mathcal{O}(h^{M+2}), & h &\rightarrow 0, \\ -c_{-1}(h)E_1(-h) + c_1(h)E_1(h) &= \mathcal{O}(h^{M+1}), & h &\rightarrow 0. \end{aligned}$$

Solving the above equation and noting that $E_0(0) = E_1(0) = 1$, we conclude that (3.6) holds if and only if (3.8) holds. Thus, (3.8) holds for numerical dispersion order M if and only if (3.6) holds.

Next, we tackle the accuracy order in (3.9). Since we proved (3.8) and $M \geq \tilde{M}$, (3.9) holds for accuracy order \tilde{M} if and only if all the coefficients of $f_0, \dots, f_{\tilde{M}-1}$ must be $\mathcal{O}(h^{\tilde{M}+2})$ as $h \rightarrow 0$. Rearranging the last line of (3.10), we conclude

$$\sum_{\ell=0}^{\infty} h^{\ell+2} \left(c_1(h)F_\ell(h) + (-1)^\ell c_{-1}(h)F_\ell(-h) \right) f_\ell - (d_0 + 1)h^2 f_0 - \sum_{\ell=1}^{\tilde{M}-1} d_\ell h^{\ell+2} f_\ell$$

$$= \sum_{\ell=0}^{\tilde{M}-1} h^{\ell+2} \left(-(d_\ell + \delta_{0,\ell}) + c_1(h)F_\ell(h) + (-1)^\ell c_{-1}(h)F_\ell(-h) \right) f_\ell + \mathcal{O}(h^{\tilde{M}+2}).$$

Since (3.8) holds, (3.9) now is equivalent to that all the coefficients f_ℓ , $\ell = 0, \dots, \tilde{M} - 1$ in the above identity must be $\mathcal{O}(h^{\tilde{M}+2})$, that is,

$$-(d_\ell + \delta_{0,\ell}) + c_1(h)F_\ell(h) + (-1)^\ell c_{-1}(h)F_\ell(-h) = \mathcal{O}(h^{\tilde{M}-\ell}), \quad \ell = 0, \dots, \tilde{M} - 1.$$

Solving the above linear equations for $d_0, \dots, d_{\tilde{M}-1}$ and using (3.6), we obtain (3.7). This proves (3.9) for accuracy order \tilde{M} . \square

We make some remarks on Theorem 3.2. First of all, from the proof of Theorem 3.2, we see that Theorem 3.2 finds all the possible compact finite difference schemes with accuracy order \tilde{M} and numerical dispersion order M . Because (3.9) for accuracy order \tilde{M} automatically implies (3.8) for numerical dispersion order M with $M = \tilde{M}$, we often take $M = \tilde{M}$. For example, for $M = \tilde{M} \in 2\mathbb{N}$, one particular choice of c_{-1}, c_0, c_1 satisfying (3.6) is

$$c_{-1}(h) := -\mathcal{E}_1^{M-1}(-h), \quad c_1(h) := -\mathcal{E}_1^{M-1}(h), \quad c_0(h) := \mathcal{E}_1^{M-1}(h)\mathcal{E}_0^M(h) + \mathcal{E}_1^{M-1}(-h)\mathcal{E}_0^M(-h), \quad (3.11)$$

and the corresponding d_ℓ , $\ell = 0, \dots, M - 2$ are given by

$$d_\ell(h) := -\delta_{0,\ell} - \mathcal{E}_1^{M-1}(h)\mathcal{F}_\ell^{M-\ell-2}(h) - (-1)^\ell \mathcal{E}_1^{M-1}(-h)\mathcal{F}_\ell^{M-\ell-2}(-h), \quad (3.12)$$

where $\mathcal{E}_0^n, \mathcal{E}_1^n, \mathcal{F}_\ell^n$, $n \in \mathbb{N}$ are the unique polynomials (in terms of h) of degree n satisfying

$$\mathcal{E}_0^n(h) = E_0(h) + \mathcal{O}(h^{n+1}), \quad \mathcal{E}_1^n(h) := 1/E_1(h) + \mathcal{O}(h^{n+1}), \quad \mathcal{F}_\ell^n(h) = F_\ell(h) + \mathcal{O}(h^{n+1}), \quad (3.13)$$

as $h \rightarrow 0$. Notice that $d_{M-1}(h) = 0$ and $E_1(0) = 1$. Observing $c_1(h) + (-1)^{M-1}c_{-1}(h) = \mathcal{O}(h)$ for even $M \in 2\mathbb{N}$, one can directly check that the above choice in (3.11) and (3.12) satisfies all the conditions in (3.6) and (3.7) with $\alpha(h) = 1 - \beta h^M$, where β is the coefficient of h^M in the Taylor series of $\frac{1}{E_1(h)}$ at $h = 0$. Note that c_{-1}, c_0, c_1 in (3.11) and d_ℓ , $\ell = 0, \dots, M - 2$ in (3.12) only depend on $a, a', \dots, a^{(M-1)}, \kappa^2, [\kappa^2]', \dots, [\kappa^2]^{(M-2)}$ and $f, f', \dots, f^{(M-2)}$. Secondly, if E_0 and E_1 in (3.3) have closed forms, then we can have numerical dispersion order $M = \infty$ for a pollution free scheme by selecting $c_1(h) = -1/E_1(h)$, $c_{-1}(h) = -1/E_1(-h)$ and $c_0(h) = E_0(h)/E_1(h) + E_0(-h)/E_1(-h)$ in (3.6). In particular, for constant functions a and κ^2 , we observe

$$E_0(h) = \cos(\tilde{h}), \quad E_1(h) = \frac{\sin(\tilde{h})}{\tilde{h}} \quad \text{with} \quad \tilde{h} := h\kappa/\sqrt{a} \quad (3.14)$$

and for $\ell \in \mathbb{N}_0$,

$$F_{2\ell}(h) = \frac{\cos(\tilde{h}) - \sum_{j=0}^{\ell} \frac{(-1)^j \tilde{h}^{2j}}{(2j)!}}{a(-1)^{\ell+1} \tilde{h}^{2\ell+2}}, \quad F_{2\ell+1}(h) = \frac{\sin(\tilde{h}) - \sum_{j=0}^{\ell} \frac{(-1)^j \tilde{h}^{2j+1}}{(2j+1)!}}{a(-1)^{\ell+1} \tilde{h}^{2\ell+3}}. \quad (3.15)$$

Thirdly, if both a and κ^2 are real-valued smooth functions, then all coefficients $c_{-1}(h), c_0(h), c_1(h)$ and $d_\ell(h)$, $\ell = 0, \dots, M - 2$ are real numbers in (3.11) and (3.12).

3.2. Compact stencils for boundary points. We now handle the case that the base point is one of the endpoints. It is important that the compact finite difference scheme should achieve the same accuracy order and numerical dispersion order at the endpoints as it does at interior points for any given boundary conditions in (2.2). The following result answers this question. For simplicity, we only handle the boundary condition at a base point x_b from its right side, while the treatment for the boundary condition at x_b from its left side is similar through symmetry. Because we shall handle piecewise smooth coefficients, let us consider a general boundary condition at $x_b \in [0, 1)$ from its right side. For $j \in \mathbb{N}_0$ and a function $f(x)$, $f^{(j)}(x_b+) := \lim_{x \rightarrow x_b^+} f^{(j)}(x)$ and $f^{(j)}(x_b-) := \lim_{x \rightarrow x_b^-} f^{(j)}(x)$ for one-sided derivatives.

Theorem 3.3. *Suppose that a, κ^2, f in (2.1) are smooth functions. Let M, \tilde{M} be positive integers with $M \geq \tilde{M}$. Let $0 < h < 1$ and the boundary condition at $x_b \in [0, 1)$ with $(x_b, x_b + h) \subset (0, 1)$. Suppose that the boundary condition at x_b for the right side of x_b is given by*

$$\mathcal{B}^+ u(x_b) := \lambda_0 u(x_b+) + \lambda_1 u'(x_b+) \quad \text{with} \quad \lambda_0, \lambda_1 \in \mathbb{C}. \quad (3.16)$$

Consider the discretization stencil of a compact finite difference scheme for $\mathcal{L}u := [a(x)u'(x)]' + \kappa^2(x)u(x) = f(x)$ at the base point x_b , from the right side of x_b with the above boundary condition, below

$$\mathcal{L}_h^{\mathcal{B}^+} u(x_b) := h^{-1} [c_0^{\mathcal{B}^+}(h)u(x_b) + c_1^{\mathcal{B}^+}(h)u(x_b + h)] - \sum_{\ell=0}^{\tilde{M}-1} d_\ell^{\mathcal{B}^+}(h)h^\ell f^{(\ell)}(x_b+), \quad (3.17)$$

where $c_0^{\mathcal{B}^+}, c_1^{\mathcal{B}^+}$ and $d_\ell^{\mathcal{B}^+}$ are smooth functions of h for $\ell = 0, \dots, \tilde{M} - 1$. Suppose that

$$c_1^{\mathcal{B}^+}(h) = \frac{\lambda_1}{E_1(h)} + \mathcal{O}(h^M), \quad c_0^{\mathcal{B}^+}(h) = h\lambda_0 - c_1^{\mathcal{B}^+}(h)E_0(h) + \mathcal{O}(h^{M+1}) \quad (3.18)$$

and

$$d_\ell^{\mathcal{B}^+}(h) = hc_1^{\mathcal{B}^+}(h)F_\ell(h) + \mathcal{O}(h^{\tilde{M}-\ell}), \quad \ell = 0, \dots, \tilde{M} - 1, \quad (3.19)$$

as $h \rightarrow 0$, where $E_0, E_1, F_\ell, \ell \in \mathbb{N}_0$ are given in (3.3) of Proposition 3.1 and are determined by $a^{(n)}(x_b+)$ and $[\kappa^2]^{(n)}(x_b+)$ for $n \in \mathbb{N}_0$. Then the discretization stencil of the compact finite difference scheme at the base point x_b with the boundary condition in (3.16) from the right side of x_b satisfies

$$c_0^{\mathcal{B}^+}(h)u(x_b) + c_1^{\mathcal{B}^+}(h)u(x_b + h) = \mathcal{O}(h^M), \quad h \rightarrow 0 \quad (3.20)$$

for every solution u of $\mathcal{L}u = 0$, and

$$\mathcal{L}_h^{\mathcal{B}^+} u(x_b) - \mathcal{B}^+ u(x_b) = \mathcal{O}(h^{\tilde{M}}), \quad h \rightarrow 0 \quad (3.21)$$

for every solution u of $\mathcal{L}u = f$.

Proof. The proof is similar to the proof of Theorem 3.2. Using (3.2), we have

$$\begin{aligned} h\mathcal{L}_h^{\mathcal{B}^+} u(x_b) - h\mathcal{B}^+ u(x_b) &= u_0 \left(c_0^{\mathcal{B}^+}(h) + E_0(h)c_1^{\mathcal{B}^+}(h) - h\lambda_0 \right) + u_1 \left(hE_1(h)c_1^{\mathcal{B}^+}(h) - h\lambda_1 \right) \\ &\quad + \sum_{\ell=0}^{\infty} h^{\ell+2} f_\ell c_1^{\mathcal{B}^+}(h)F_\ell(h) - \sum_{\ell=0}^{\tilde{M}-1} d_\ell^{\mathcal{B}^+}(h)h^{\ell+1}f_\ell, \end{aligned}$$

where $u_0 := u(x_b), u_1 := u'(x_b)$ and $f_\ell := f^{(\ell)}(x_b+)$. Then (3.20) holds for numerical dispersion order M if and only if

$$c_0^{\mathcal{B}^+}(h) + E_0(h)c_1^{\mathcal{B}^+}(h) - h\lambda_0 = \mathcal{O}(h^{M+1}), \quad E_1(h)c_1^{\mathcal{B}^+}(h) - \lambda_1 = \mathcal{O}(h^M),$$

as $h \rightarrow 0$. Noting that $E_1(0) = E_0(0) = 1$, we conclude that the above equations hold if and only if (3.18) holds. Since (3.18) holds and $M \geq \tilde{M}$, to have accuracy order \tilde{M} , the coefficients of f_ℓ must be $\mathcal{O}(h^{\tilde{M}+1})$. That is,

$$-d_\ell^{\mathcal{B}^+}(h) + c_1^{\mathcal{B}^+}(h)hF_\ell(h) = \mathcal{O}(h^{\tilde{M}-\ell}), \quad h \rightarrow 0, \quad \ell = 0, \dots, \tilde{M} - 1.$$

Solving the above equations for $d_\ell^{\mathcal{B}^+}$, we obtain (3.19). \square

We make some remarks on Theorem 3.3. If E_0 and E_1 in (3.3) have closed forms, then we can achieve numerical dispersion order $M = \infty$ for pollution free by selecting $c_1(h) = \frac{\lambda_1}{E_1(h)}$ and $c_0(h) = h\lambda_0 - \frac{E_0(h)}{E_1(h)}\lambda_1$. In particular, for constant functions a and κ^2 , E_0, E_1, F_ℓ are given in (3.14) and (3.15). For $M = \tilde{M} \in 2\mathbb{N}$, one particular choice of $c_1^{\mathcal{B}^+}$ and $c_0^{\mathcal{B}^+}$ are given by

$$c_1^{\mathcal{B}^+}(h) := -\lambda_1 \mathcal{E}_1^{M-1}(h), \quad c_0^{\mathcal{B}^+}(h) := h\lambda_0 + \lambda_1 \mathcal{E}_1^{M-1}(h) \mathcal{E}_0^M(h), \quad (3.22)$$

and their corresponding $d_\ell^{\mathcal{B}^+}$, $\ell = 0, \dots, M-1$ are given by $d_{M-1}^{\mathcal{B}^+}(h) = 0$ and

$$d_\ell^{\mathcal{B}^+}(h) = -h\lambda_1 \mathcal{E}_1^{M-1}(h) \mathcal{F}_\ell^{M-\ell-2}(h), \quad \ell = 0, \dots, M-2, \quad (3.23)$$

where $\mathcal{E}_0^n, \mathcal{E}_1^n, F_\ell^n, n \in \mathbb{N}$ are defined in (3.13).

Similarly, let the boundary condition at x_b for the left side of x_b is given by

$$\mathcal{B}^- u(x_b) := \lambda_0 u(x_b-) + \lambda_1 u'(x_b-) \quad \text{with} \quad \lambda_0, \lambda_1 \in \mathbb{C}.$$

Then the discretization stencil for $\mathcal{L}u := [a(x)u'(x)]' + \kappa^2(x)u(x) = f(x)$ at the base point x_b from the left side of x_b

$$\mathcal{L}_h^{\mathcal{B}^-} u(x_b) := h^{-1} [c_{-1}^{\mathcal{B}^-}(h)u(x_b - h) + c_0^{\mathcal{B}^-}(h)u(x_b)] - \sum_{\ell=0}^{\tilde{M}-1} d_\ell^{\mathcal{B}^-}(h) h^\ell f^{(\ell)}(x_b-)$$

satisfies the corresponding relations in (3.20) and (3.21) if

$$c_{-1}^{\mathcal{B}^-}(h) = -\frac{\lambda_1}{E_1(-h)} + \mathcal{O}(h^M), \quad c_0^{\mathcal{B}^-}(h) = h\lambda_0 - c_{-1}^{\mathcal{B}^-}(h)E_0(-h) + \mathcal{O}(h^{M+1}), \quad h \rightarrow 0$$

and

$$d_\ell^{\mathcal{B}^-}(h) = hc_{-1}^{\mathcal{B}^-}(h)(-1)^\ell F_\ell(-h) + \mathcal{O}(h^{\tilde{M}-\ell}), \quad h \rightarrow 0.$$

In other words,

$$c_{-1}^{\mathcal{B}^-}(h) = -c_1^{\mathcal{B}^+}(-h), \quad c_0^{\mathcal{B}^-}(h) = -c_0^{\mathcal{B}^+}(-h) \quad \text{and} \quad d_\ell^{\mathcal{B}^-}(h) = (-1)^\ell d_\ell^{\mathcal{B}^+}(-h), \quad \ell \in \mathbb{N}_0. \quad (3.24)$$

3.3. Compact stencils for piecewise smooth coefficients. We now discuss how to use the compact finite difference schemes with high accuracy order in Subsections 3.1 and 3.2 to deal with piecewise smooth coefficients a, κ^2 and f . For simplicity, we assume that a, κ^2, f are smooth for all $x > x_b$ and all $x < x_b$, but they may be discontinuous at the base point x_b . We also assume that all the one-sided derivatives of a, κ, f exist at x_b . Now define boundary operators at x_b by

$$\mathcal{B}^+ u(x_b) := u'(x_b+) \quad \text{and} \quad \mathcal{B}^- u(x_b) := u'(x_b-). \quad (3.25)$$

Using Theorem 3.3 with $\lambda_0 = 0$ and $\lambda_1 = 1$, we can construct discretization stencils $\mathcal{L}_h^{\mathcal{B}^+} u(x_b)$ (using one-sided derivatives of a, κ^2, f from the right side of x_b) and $\mathcal{L}_h^{\mathcal{B}^-} u(x_b)$ (using one-sided derivatives of a, κ^2, f from the left side of x_b) such that they have accuracy order \tilde{M} and numerical dispersion order M . We assume that the source term f contains a Dirac distribution $w\delta_{x_b}$ at the point x_b with weight $w \in \mathbb{C}$. Then it is well known that the solution u to (2.1) with boundary conditions in (2.2) must satisfy $a(x_b+)u'(x_b+) - a(x_b-)u'(x_b-) = w$. Therefore, at the base point x_b , we obtain the discretization stencil

$$\mathcal{L}_h u = a(x_b+)\mathcal{L}_h^{\mathcal{B}^+} u(x_b) - a(x_b-)\mathcal{L}_h^{\mathcal{B}^-} u(x_b) = w$$

at the base point x_b , where a, κ^2, f may be discontinuous. This above compact scheme will be also used to solve the Dirac-assisted local problems of (2.10) in DAT.

Next we discuss how to estimate u' with high accuracy order at knot points. Let $0 = x_0 < x_1 < \dots < x_N = 1$ be a mesh such that $x_{j+1} - x_j = \mathcal{O}(h)$ uniformly for all $j = 0, \dots, N-1$. Let us denote the numerical solution by $\{u(x_j)\}_{j=0}^N$ of the heterogeneous Helmholtz equation in (2.1)–(2.2) using our developed compact finite difference scheme with accuracy order M . Let u_e be the exact solution and x_b be one of $\{x_j\}_{j=0}^N$. Then we know that $u(x_b) = u_e(x_b) + \mathcal{O}(h^M)$ as $h \rightarrow 0$. We can estimate $u'(x_b)$ with accuracy order M as well. Basically, let $\mathcal{L}_h^{\mathcal{B}^+} u(x_b)$ and $\mathcal{L}_h^{\mathcal{B}^-} u(x_b)$ be the stencils with accuracy order M for boundary conditions in (3.25). Then we have

$$u'_e(x_b+) = \mathcal{L}_h^{\mathcal{B}^+} u(x_b) + \mathcal{O}(h^M), \quad u'_e(x_b-) = \mathcal{L}_h^{\mathcal{B}^-} u(x_b) + \mathcal{O}(h^M), \quad h \rightarrow 0. \quad (3.26)$$

Therefore, the one-sided derivatives of the exact solution u_e at x_b can be estimated by $\mathcal{L}_h^{\mathcal{B}^+} u(x_b)$ and $\mathcal{L}_h^{\mathcal{B}^-} u(x_b)$ with accuracy order M . We point out that higher order derivatives at x_b can also be estimated with accuracy order M thanks to Proposition 3.1. Moreover, since we can obtain the derivatives of u_e at all knot points with accuracy order M , using interpolation we can obtain

a function $u(x), 0 \leq x \leq 1$ from the computed discrete data $\{u(x_j)\}_{j=0}^N$ such that the function u accurately approximates the exact solution u_e in the function setting. The identities in (3.26) play a critical role in DAT to estimate artificial Dirac distributions in (2.9) and (2.12) with high accuracy order. The identities in (3.26) will be also used in the coming section on numerical experiments to calculate the convergence rates in the relative H^1 energy norm. We shall also observe in the next section that DAT coupled with the compact finite difference scheme of accuracy order M ($M = 6, 8$ in Section 4), the convergence rates, in relative L_2, L_∞ , and H^1 energy norms, are also of order M .

3.4. A concrete example with accuracy order 8. For the convenience of the reader, here we provide concrete compact finite difference schemes with M -th order accuracy and numerical dispersion, where $M = 2, 4, 6, 8$. Note that $a_j := a^{(j)}(x_b)$, $f_j := f^{(j)}(x_b)$ and $\kappa_j := [\kappa^2]^{(j)}(x_b)$, where $x_b \in [0, 1]$. Recall that the stencil for interior points is given in (3.11) with $M = 8$, that is,

$$c_{-1}(h) := -\mathcal{E}_1^7(-h), \quad c_1(h) := -\mathcal{E}_1^7(h), \quad c_0(h) := \mathcal{E}_1^7(h)\mathcal{E}_0^8(h) + \mathcal{E}_1^7(-h)\mathcal{E}_0^8(-h), \quad (3.27)$$

where \mathcal{E}_1^7 and \mathcal{E}_0^8 are defined in (3.13) and are explicitly given by

$$\begin{aligned} \mathcal{E}_1^7 = & -1 - \frac{ha_1}{2a_0} - (2a_0a_2 + 2a_0\kappa_0 - a_1^2) \frac{h^2}{12a_0^2} - (a_3a_0^2 + 2\kappa_1a_0^2 - 2a_1a_2a_0 + a_1^3) \frac{h^3}{24a_0^3} - (6a_4a_0^3 + 18\kappa_2a_0^3 \\ & - 18a_1a_3a_0^2 - 6a_1\kappa_1a_0^2 - 16a_2^2a_0^2 - 2a_2\kappa_0a_0^2 + 14\kappa_0^2a_0^2 + 46a_1^2a_2a_0 - 2a_1^2\kappa_0a_0 - 19a_1^4) \frac{h^4}{720a_0^4} - (2a_5a_0^4 \\ & + 8\kappa_3a_0^4 - 8a_1a_4a_0^3 - 6a_1\kappa_2a_0^3 - 20a_2a_3a_0^3 - 8a_2\kappa_1a_0^3 - 2a_3\kappa_0a_0^3 + 28\kappa_0\kappa_1a_0^3 + 29a_1^2a_3a_0^2 + 4a_1^2\kappa_1a_0^2 \\ & + 48a_1a_2^2a_0^2 - 2a_1a_2\kappa_0a_0^2 - 14a_1\kappa_0^2a_0^2 - 78a_1^3a_2a_0 + 4a_1^3\kappa_0a_0 + 27a_1^5) \frac{h^5}{1440a_0^5} - (12a_6a_0^5 + 60\kappa_4a_0^5 \\ & - 60a_1a_5a_0^4 - 72a_1\kappa_3a_0^4 - 192a_2a_4a_0^4 - 156a_2\kappa_2a_0^4 - 135a_3^2a_0^4 - 120a_3\kappa_1a_0^4 - 24a_4\kappa_0a_0^4 + 348\kappa_0\kappa_2a_0^4 \\ & + 300\kappa_1^2a_0^4 + 282a_1^2a_4a_0^3 + 114a_1^2\kappa_2a_0^3 + 1296a_1a_2a_3a_0^3 + 204a_1a_2\kappa_1a_0^3 - 708a_1\kappa_0\kappa_1a_0^3 + 352a_2^3a_0^3 \\ & - 12a_2^2\kappa_0a_0^3 - 240a_2\kappa_0^2a_0^3 + 124\kappa_0^3a_0^3 - 1056a_1^3a_3a_0^2 - 66a_1^3\kappa_1a_0^2 - 2544a_1^2a_2^2a_0^2 + 198a_1^2a_2\kappa_0a_0^2 \\ & + 354a_1^2\kappa_0^2a_0^2 + 2910a_1^4a_2a_0 - 150a_1^4\kappa_0a_0 - 863a_1^6) \frac{h^6}{60480a_0^6} - (3a_7a_0^6 + 18\kappa_5a_0^6 - 18a_1a_6a_0^5 - 30a_1\kappa_4a_0^5 \\ & - 70a_2a_5a_0^5 - 88a_2\kappa_3a_0^5 - 126a_3a_4a_0^5 - 108a_3\kappa_2a_0^5 - 60a_4\kappa_1a_0^5 - 10a_5\kappa_0a_0^5 + 152\kappa_0\kappa_3a_0^5 + 360\kappa_1\kappa_2a_0^5 \\ & + 104a_1^2a_5a_0^4 + 74a_1^2\kappa_3a_0^4 + 610a_1a_2a_4a_0^4 + 252a_1a_2\kappa_2a_0^4 + 423a_1a_3^2a_0^4 + 156a_1a_3\kappa_1a_0^4 + 10a_1a_4\kappa_0a_0^4 \\ & - 468a_1\kappa_0\kappa_2a_0^4 - 420a_1\kappa_1^2a_0^4 + 686a_2^2a_3a_0^4 + 108a_2^2\kappa_1a_0^4 + 4a_2a_3\kappa_0a_0^4 - 600a_2\kappa_0\kappa_1a_0^4 - 142a_3\kappa_0^2a_0^4 \\ & + 372\kappa_0^2\kappa_1a_0^4 - 500a_1^3a_4a_0^3 - 126a_1^3\kappa_2a_0^3 - 3316a_1^2a_2a_3a_0^3 - 240a_1^2a_2\kappa_1a_0^3 + 86a_1^2a_3\kappa_0a_0^3 + 948a_1^2\kappa_0\kappa_1a_0^3 \\ & - 1760a_1a_2^3a_0^3 + 168a_1a_2^2\kappa_0a_0^3 + 600a_1a_2\kappa_0^2a_0^3 - 248a_1\kappa_0^3a_0^3 + 1899a_1^4a_3a_0^2 + 48a_1^4\kappa_1a_0^2 + 6000a_1^3a_2^2a_0^2 \\ & - 522a_1^3a_2\kappa_0a_0^2 - 474a_1^3\kappa_0^2a_0^2 - 5310a_1^5a_2a_0 + 264a_1^5\kappa_0a_0 + 1375a_1^7) \frac{h^7}{120960a_0^7}, \end{aligned}$$

and

$$\begin{aligned} \mathcal{E}_0^8 = & 1 - \frac{\kappa_0h^2}{2a_0} + (-\kappa_1a_0 + 2a_1\kappa_0) \frac{h^3}{6a_0^2} + (-\kappa_2a_0^2 + 3a_1\kappa_1a_0 + 3a_2\kappa_0a_0 + \kappa_0^2a_0 - 6a_1^2\kappa_0) \frac{h^4}{24a_0^3} \\ & + (-\kappa_3a_0^3 + 4a_1\kappa_2a_0^2 + 6a_2\kappa_1a_0^2 + 4a_3\kappa_0a_0^2 + 4\kappa_0\kappa_1a_0^2 - 12a_1^2\kappa_1a_0 - 24a_1a_2\kappa_0a_0 - 6a_1\kappa_0^2a_0 \\ & + 24a_1^3\kappa_0) \frac{h^5}{120a_0^4} + (-\kappa_4a_0^4 + 5a_1\kappa_3a_0^3 + 10a_2\kappa_2a_0^3 + 10a_3\kappa_1a_0^3 + 5a_4\kappa_0a_0^3 + 7\kappa_0\kappa_2a_0^3 \\ & + 4\kappa_1^2a_0^3 - 20a_1^2\kappa_2a_0^2 - 60a_1a_2\kappa_1a_0^2 - 40a_1a_3\kappa_0a_0^2 - 31a_1\kappa_0\kappa_1a_0^2 - 30a_2^2\kappa_0a_0^2 - 13a_2\kappa_0^2a_0^2 \\ & - \kappa_0^3a_0^2 + 60a_1^3\kappa_1a_0 + 180a_1^2a_2\kappa_0a_0 + 36a_1^2\kappa_0^2a_0 - 120a_1^4\kappa_0) \frac{h^6}{720a_0^5} + (-\kappa_5a_0^5 + 6a_1\kappa_4a_0^4 \\ & + 15a_2\kappa_3a_0^4 + 20a_3\kappa_2a_0^4 + 15a_4\kappa_1a_0^4 + 6a_5\kappa_0a_0^4 + 11\kappa_0\kappa_3a_0^4 + 15\kappa_1\kappa_2a_0^4 - 30a_1^2\kappa_3a_0^3 - 120a_1a_2\kappa_2a_0^3 \\ & - 120a_1a_3\kappa_1a_0^3 - 60a_1a_4\kappa_0a_0^3 - 66a_1\kappa_0\kappa_2a_0^3 - 39a_1\kappa_1^2a_0^3 - 90a_2^2\kappa_1a_0^3 - 120a_2a_3\kappa_0a_0^3 - 81a_2\kappa_0\kappa_1a_0^3 \end{aligned}$$

$$\begin{aligned}
& -24a_3\kappa_0^2a_0^3 - 9\kappa_0^2\kappa_1a_0^3 + 120a_1^3\kappa_2a_0^2 + 540a_1^2a_2\kappa_1a_0^2 + 360a_1^2a_3\kappa_0a_0^2 + 228a_1^2\kappa_0\kappa_1a_0^2 + 540a_1a_2^2\kappa_0a_0^2 \\
& + 192a_1a_2\kappa_0^2a_0^2 + 12a_1\kappa_0^3a_0^2 - 360a_1^4\kappa_1a_0 - 1440a_1^3a_2\kappa_0a_0 - 240a_1^3\kappa_0^2a_0 + 720a_1^5\kappa_0) \frac{h^7}{5040a_0^6} + (-\kappa_6a_0^6 \\
& + 7a_1\kappa_5a_0^5 + 21a_2\kappa_4a_0^5 + 35a_3\kappa_3a_0^5 + 35a_4\kappa_2a_0^5 + 21a_5\kappa_1a_0^5 + 7a_6\kappa_0a_0^5 + 16\kappa_0\kappa_4a_0^5 + 26\kappa_1\kappa_3a_0^5 \\
& + 15\kappa_2^2a_0^5 - 42a_1^2\kappa_4a_0^4 - 210a_1a_2\kappa_3a_0^4 - 280a_1a_3\kappa_2a_0^4 - 210a_1a_4\kappa_1a_0^4 - 84a_1a_5\kappa_0a_0^4 - 122a_1\kappa_0\kappa_3a_0^4 \\
& - 174a_1\kappa_1\kappa_2a_0^4 - 210a_2^2\kappa_2a_0^4 - 420a_2a_3\kappa_1a_0^4 - 210a_2a_4\kappa_0a_0^4 - 202a_2\kappa_0\kappa_2a_0^4 - 120a_2\kappa_1^2a_0^4 - 140a_3^2\kappa_0a_0^4 \\
& - 174a_3\kappa_0\kappa_1a_0^4 - 40a_4\kappa_0^2a_0^4 - 22\kappa_0^2\kappa_2a_0^4 - 28\kappa_0\kappa_1^2a_0^4 + 210a_1^3\kappa_3a_0^3 + 1260a_1^2a_2\kappa_2a_0^3 + 1260a_1^2a_3\kappa_1a_0^3 \\
& + 630a_1^2a_4\kappa_0a_0^3 + 572a_1^2\kappa_0\kappa_2a_0^3 + 345a_1^2\kappa_1^2a_0^3 + 1890a_1a_2^2\kappa_1a_0^3 + 2520a_1a_2a_3\kappa_0a_0^3 + 1422a_1a_2\kappa_0\kappa_1a_0^3 \\
& + 418a_1a_3\kappa_0^2a_0^3 + 130a_1\kappa_0^2\kappa_1a_0^3 + 630a_2^3\kappa_0a_0^3 + 303a_2^2\kappa_0^2a_0^3 + 34a_2\kappa_0^3a_0^3 + \kappa_0^4a_0^3 - 840a_1^4\kappa_2a_0^2 \\
& - 5040a_1^3a_2\kappa_1a_0^2 - 3360a_1^3a_3\kappa_0a_0^2 - 1800a_1^3\kappa_0\kappa_1a_0^2 - 7560a_1^2a_2^2\kappa_0a_0^2 - 2280a_1^2a_2\kappa_0^2a_0^2 - 120a_1^2\kappa_0^3a_0^2 \\
& + 2520a_1^5\kappa_1a_0 + 12600a_1^4a_2\kappa_0a_0 + 1800a_1^4\kappa_0^2a_0 - 5040a_1^6\kappa_0) \frac{h^8}{40320a_0^7}.
\end{aligned}$$

Their corresponding $d_\ell(h)$, $\ell = 0, \dots, 6$ are given in (3.12) with $M = 8$ and

$$\begin{aligned}
\mathcal{F}_0^6(h) &= \frac{1}{2a_0} - \frac{a_1h}{3a_0^2} + (-3a_2a_0 - \kappa_0a_0 + 6a_1^2) \frac{h^2}{24a_0^3} + (-4a_3a_0^2 - 3\kappa_1a_0^2 + 24a_1a_2a_0 + 6a_1\kappa_0a_0 \\
& - 24a_1^3) \frac{h^3}{120a_0^4} + (-5a_4a_0^3 - 6\kappa_2a_0^3 + 40a_1a_3a_0^2 + 23a_1\kappa_1a_0^2 + 30a_2^2a_0^2 + 13a_2\kappa_0a_0^2 + \kappa_0^2a_0^2 \\
& - 180a_1^2a_2a_0 - 36a_1^2\kappa_0a_0 + 120a_1^4) \frac{h^4}{720a_0^5} + (-3a_0^4a_5 - 5a_0^4\kappa_3 + 30a_0^3a_1a_4 + 28a_0^3a_1\kappa_2 \\
& + 60a_0^3a_2a_3 + 30a_0^3a_2\kappa_1 + 12a_0^3a_3\kappa_0 + 4a_0^3\kappa_0\kappa_1 - 180a_0^2a_1^2a_3 - 84a_0^2a_1^2\kappa_1 - 270a_0^2a_1a_2^2 \\
& - 96a_0^2a_1a_2\kappa_0 - 6a_0^2a_1\kappa_0^2 + 720a_0a_1^3a_2 + 120a_0a_1^3\kappa_0 - 360a_1^5) \frac{h^5}{2520a_0^6} + (-7a_0^5a_6 - 15a_0^5\kappa_4 \\
& + 84a_0^4a_1a_5 + 110a_0^4a_1\kappa_3 + 210a_0^4a_2a_4 + 171a_0^4a_2\kappa_2 + 140a_0^4a_3^2 + 129a_0^4a_3\kappa_1 + 40a_0^4a_4\kappa_0 \\
& + 21a_0^4\kappa_0\kappa_2 + 18a_0^4\kappa_1^2 - 630a_0^3a_1^2a_4 - 482a_0^3a_1^2\kappa_2 - 2520a_0^3a_1a_2a_3 - 1047a_0^3a_1a_2\kappa_1 \\
& - 418a_0^3a_1a_3\kappa_0 - 115a_0^3a_1\kappa_0\kappa_1 - 630a_0^3a_2^3 - 303a_0^3a_2^2\kappa_0 - 34a_0^3a_2\kappa_0^2 - a_0^3\kappa_0^3 + 3360a_0^2a_1^3a_3 \\
& + 1320a_0^2a_1^3\kappa_1 + 7560a_0^2a_1^2a_2^2 + 2280a_0^2a_1^2a_2\kappa_0 + 120a_0^2a_1^2\kappa_0^2 - 12600a_0a_1^4a_2 - 1800a_0a_1^4\kappa_0 \\
& + 5040a_1^6) \frac{h^6}{40320a_0^7}, \\
\mathcal{F}_1^5(h) &= \frac{1}{6a_0} - \frac{a_1h}{8a_0^2} + (-6a_2a_0 - \kappa_0a_0 + 12a_1^2) \frac{h^2}{120a_0^3} + (-5a_3a_0^2 - 2\kappa_1a_0^2 + 30a_1a_2a_0 + 4a_1\kappa_0a_0 \\
& - 30a_1^3) \frac{h^3}{360a_0^4} + (-15a_0^4a_4 - 10a_0^4\kappa_2 + 120a_0^3a_1a_3 + 39a_0^3a_1\kappa_1 + 90a_0^3a_2^2 + 21a_0^3a_2\kappa_0 + a_0^3\kappa_0^2 \\
& - 540a_0^2a_1^2a_2 - 60a_0^2a_1^2\kappa_0 + 360a_0a_1^4) \frac{h^4}{5040a_0^5} + (-21a_0^5a_5 - 20a_0^5\kappa_3 + 210a_0^4a_1a_4 + 115a_0^4a_1\kappa_2 \\
& + 420a_0^4a_2a_3 + 120a_0^4a_2\kappa_1 + 45a_0^4a_3\kappa_0 + 10a_0^4\kappa_0\kappa_1 - 1260a_0^3a_1^2a_3 - 345a_0^3a_1^2\kappa_1 - 1890a_0^3a_1a_2^2 \\
& - 375a_0^3a_1a_2\kappa_0 - 15a_0^3a_1\kappa_0^2 + 5040a_0^2a_1^3a_2 + 480a_0^2a_1^3\kappa_0 - 2520a_0a_1^5) \frac{h^5}{40320a_0^7}, \\
\mathcal{F}_2^4(h) &= \frac{1}{24a_0} - \frac{a_1h}{30a_0^2} + (-10a_2a_0 - \kappa_0a_0 + 20a_1^2) \frac{h^2}{720a_0^3} + (-4a_0^4a_3 - a_0^4\kappa_1 + 24a_0^3a_1a_2 + 2a_0^3a_1\kappa_0 \\
& - 24a_0^2a_1^3) \frac{h^3}{1008a_0^6} + (-35a_0^5a_4 - 15a_0^5\kappa_2 + 280a_0^4a_1a_3 + 59a_0^4a_1\kappa_1 + 210a_0^4a_2^2 + 31a_0^4a_2\kappa_0
\end{aligned}$$

$$\begin{aligned}
& + a_0^4 \kappa_0^2 - 1260 a_0^3 a_1^2 a_2 - 90 a_0^3 a_1^2 \kappa_0 + 840 a_0^2 a_1^4 \frac{h^4}{40230 a_0^7}, \\
\mathcal{F}_3^3(h) &= \frac{1}{120 a_0} - \frac{a_1 h}{144 a_0^2} + (-15 a_0^4 a_2 - a_0^4 \kappa_0 + 30 a_0^3 a_1^2) \frac{h^2}{5040 a_0^6} + (-35 a_0^5 a_3 - 6 a_0^5 \kappa_1 + 210 a_0^4 a_1 a_2 \\
& + 12 a_0^4 a_1 \kappa_0 - 210 a_0^3 a_1^3) \frac{h^3}{40320 a_0^7}, \\
\mathcal{F}_4^2(h) &= \frac{1}{720 a_0} - \frac{a_1 h}{840 a_0^2} + (-21 a_0^5 a_2 - a_0^5 \kappa_0 + 42 a_0^4 a_1^2) \frac{h^2}{40320 a_0^7}, \\
\mathcal{F}_5^1(h) &= \frac{1}{5040 a_0} - \frac{a_1 h}{5760 a_0^2}, \quad \mathcal{F}_6^0(h) = \frac{1}{40320 a_0}.
\end{aligned}$$

For the stencil used at the left boundary point or to the right of a discontinuity point as in (3.18), we take $c_1^{\mathcal{B}^+}(h) = \lambda_1 \mathcal{E}_1^7(h)$ and $c_0^{\mathcal{B}^+}(h) = h \lambda_0 - c_1^{\mathcal{B}^+}(h) \mathcal{E}_0^8(h)$. By (3.24), we obtain the stencil used at the right boundary point or to the left of a discontinuity point.

For the lower accuracy orders $M = 2, 4, 6$, the stencil for interior points is given in (3.11), that is,

$$c_{-1}(h) := -\mathcal{E}_1^{M-1}(-h), \quad c_1(h) := -\mathcal{E}_1^{M-1}(h), \quad c_0(h) := \mathcal{E}_1^{M-1}(h) \mathcal{E}_0^M(h) + \mathcal{E}_1^{M-1}(-h) \mathcal{E}_0^M(-h)$$

and d_ℓ are given in (3.12), where all polynomials $\mathcal{E}_0^M, \mathcal{E}_1^{M-1}, \mathcal{F}_\ell^{M-\ell-2}$ (see (3.13) for definition) with $M = 2, 4, 6$ can be easily obtained by truncating the above given $\mathcal{E}_0^8, \mathcal{E}_1^7, \mathcal{F}_\ell^{8-\ell-2}$ accordingly. Finally, we point out that in the above compact finite difference method with accuracy order $M \in 2\mathbb{N}$, we only need $a, a', \dots, a^{(M-1)}, \kappa^2, [\kappa^2]', \dots, [\kappa^2]^{(M-2)}$ and $f, f', \dots, f^{(M-2)}$.

4. NUMERICAL EXPERIMENTS

In this section, in addition to Example 1 we present several more numerical experiments to illustrate the performance of DAT in Section 2 and developed compact finite difference schemes in Section 3.

Let u_e and $\{u_N(x_j)\}_{j=0}^N$ be the exact (if its analytic expression is known) and approximated/computed solutions on knot points $\{x_j\}_{j=0}^N$ with $0 = x_0 < x_1 < \dots < x_{N-1} < x_N = 1$, respectively. To evaluate the performance, we shall use

$$\|u_N - u_e\|_\infty := \max_{0 \leq j \leq N} |u_N(x_j) - u_e(x_j)|, \quad \|u_N - u_e\|_2^2 := \sum_{j=0}^N h_j |u_N(x_j) - u_e(x_j)|^2, \quad (4.1)$$

where $h_j := x_{j+1} - x_j$ with convention $x_{N+1} := 1$. We can similarly define $\|u'_N - u'_e\|_\infty$ and $\|u'_N - u'_e\|_2$ by replacing u_N and u_e in (4.1) with u'_N and u'_e , respectively, where $\{u'_N(x_j)\}_{j=0}^N$ are estimated from $\{u_N(x_j)\}_{j=0}^N$ as we discussed in Subsection 3.3. Moreover, following the literature (see e.g., [15]), the energy norm is defined by

$$\| \|u_N - u_e\| \|^2 := \|\sqrt{a}(u'_N - u'_e)\|_2^2 + \|\kappa(u_N - u_e)\|_2^2. \quad (4.2)$$

We measure the performance in relative errors. When the analytic expression of the exact solution u_e is unknown, we calculate the relative error between two consecutive levels.

All condition numbers are approximated by using MATLAB's built-in function `cond`, after renormalizing all the diagonal entries to be one in the coefficient matrices. The columns ‘‘Local CN’’ and ‘‘Link CN’’ in all tables in this section list the maximum condition numbers associated with local and link problems in DAT. In fact, with a high percentage (over 90%), the condition numbers for the local and link problems in DAT are often much smaller than the maximum condition numbers listed under ‘‘Local CN’’ and ‘‘Link CN’’. The number of points used to approximate the solution is listed under ‘‘N’’. The tree level and split parameter used are denoted by ℓ and s . Unless stated otherwise, we use $s = 1$ for simplicity. In all tables, $\ell = 0$ corresponds to the result obtained from using FDM without DAT. All linear systems are solved by using MATLAB's backslash command. For each example presented below, we use the compact finite difference schemes presented in Subsection 3.4

with $M = 6, 8$. It is evident from the tables below that the 8-th order finite difference scheme always outperforms the 6-th order one. Indeed, to reach a certain error tolerance, the required number of points, N , in the 8-th order finite difference scheme is less than that of order 6.

4.1. Numerical experiments on 1D heterogeneous Helmholtz equations.

Example 2. Consider the model problem (2.1)-(2.2) given by $[a(x)u'(x)]' + \kappa^2(x)u(x) = f(x), x \in (0, 1)$ with the following coefficients

$$\begin{aligned} a &= \chi_{[0, \frac{1}{8})} + 10^{-1}\chi_{[\frac{1}{8}, \frac{2}{8})} + \chi_{[\frac{2}{8}, \frac{3}{8})} + 10^{-2}\chi_{[\frac{3}{8}, \frac{4}{8})} + \chi_{[\frac{4}{8}, \frac{5}{8})} + 10^{-3}\chi_{[\frac{5}{8}, \frac{6}{8})} + \chi_{[\frac{6}{8}, \frac{7}{8})} + 10^{-4}\chi_{[\frac{7}{8}, 1]}, \\ \kappa &= 10^4(\chi_{[0, \frac{1}{8}) \cup [\frac{2}{8}, \frac{3}{8}) \cup [\frac{4}{8}, \frac{5}{8}) \cup [\frac{6}{8}, \frac{7}{8})}) + 500(\chi_{[\frac{1}{8}, \frac{2}{8}) \cup [\frac{3}{8}, \frac{4}{8}) \cup [\frac{5}{8}, \frac{6}{8}) \cup [\frac{7}{8}, 1]}), \\ f &= 10^7 e^x(\chi_{[0, \frac{1}{8}) \cup [\frac{2}{8}, \frac{3}{8}) \cup [\frac{4}{8}, \frac{5}{8}) \cup [\frac{6}{8}, \frac{7}{8})}) - e^{-2x}(\chi_{[\frac{1}{8}, \frac{2}{8}) \cup [\frac{3}{8}, \frac{4}{8}) \cup [\frac{5}{8}, \frac{6}{8}) \cup [\frac{7}{8}, 1]}), \end{aligned}$$

and the boundary conditions $u(0) = 0$ and $10^{-2}u'(1) - i500u(1) = 0$. The exact solution u_e has an analytic expression. See Table 2 for the numerical summary as well as Figure 2 for the convergence and approximated solution plots.

N	ℓ	$\frac{\ u_N - u_e\ _\infty}{\ u_e\ _\infty}$	$\frac{\ u'_N - u'_e\ _\infty}{\ u'_e\ _\infty}$	$\frac{\ u_N - u_e\ _2}{\ u_e\ _2}$	$\frac{\ u'_N - u'_e\ _2}{\ u'_e\ _2}$	$\frac{\ u_N - u_e\ }{\ u_e\ }$	Local CN	Link CN
Accuracy order $M = 6$								
2^{15}	0	2.0833×10^{-1}	1.2491	1.6738×10^{-1}	8.1542×10^{-1}	5.8540×10^{-2}	1.6189×10^6	–
	7	2.0833×10^{-1}	1.2491	1.6738×10^{-1}	8.1542×10^{-1}	5.8540×10^{-2}	2.2686×10^4	2.3157×10^3
	10	2.0833×10^{-1}	1.2491	1.6738×10^{-1}	8.1542×10^{-1}	5.8540×10^{-2}	3.9802×10^2	2.3157×10^3
2^{16}	0	3.5328×10^{-3}	2.1422×10^{-2}	2.3941×10^{-3}	1.1795×10^{-2}	8.4201×10^{-4}	7.5545×10^6	–
	8	3.5328×10^{-3}	2.1422×10^{-2}	2.3941×10^{-3}	1.1795×10^{-2}	8.4201×10^{-4}	1.6598×10^3	2.3157×10^3
	11	3.5328×10^{-3}	2.1422×10^{-2}	2.3941×10^{-3}	1.1795×10^{-2}	8.4201×10^{-4}	1.3222×10^2	2.3157×10^3
2^{17}	0	5.1547×10^{-5}	3.1264×10^{-4}	3.4921×10^{-5}	1.7209×10^{-4}	1.2283×10^{-5}	2.8670×10^7	–
	9	5.1547×10^{-5}	3.1264×10^{-4}	3.4921×10^{-5}	1.7209×10^{-4}	1.2283×10^{-5}	1.1834×10^4	2.3157×10^3
	12	5.1547×10^{-5}	3.1264×10^{-4}	3.4921×10^{-5}	1.7209×10^{-4}	1.2283×10^{-5}	3.6510×10^1	2.3157×10^3
2^{18}	0	7.9194×10^{-7}	4.8033×10^{-6}	5.3644×10^{-7}	2.6436×10^{-6}	1.8869×10^{-7}	1.1351×10^8	–
	10	7.9194×10^{-7}	4.8033×10^{-6}	5.3644×10^{-7}	2.6436×10^{-6}	1.8869×10^{-7}	1.0867×10^4	2.3157×10^3
	13	7.9194×10^{-7}	4.8033×10^{-6}	5.3644×10^{-7}	2.6436×10^{-6}	1.8869×10^{-7}	4.2752×10^1	2.3157×10^3
2^{19}	0	1.2306×10^{-8}	7.4639×10^{-8}	8.5148×10^{-9}	4.1078×10^{-8}	3.1681×10^{-9}	4.5296×10^8	–
	11	1.2311×10^{-8}	7.4665×10^{-8}	9.3713×10^{-9}	4.1154×10^{-8}	3.3299×10^{-9}	9.3407×10^3	2.3157×10^3
	14	1.2315×10^{-8}	7.4688×10^{-8}	8.9950×10^{-9}	4.1129×10^{-8}	3.2011×10^{-9}	4.4430×10^1	2.3157×10^3
Accuracy order $M = 8$								
2^{15}	0	8.0406×10^{-3}	4.8823×10^{-2}	5.2745×10^{-3}	2.6277×10^{-2}	1.8655×10^{-3}	1.5936×10^7	–
	7	8.0406×10^{-3}	4.8823×10^{-2}	5.2745×10^{-3}	2.6277×10^{-2}	1.8655×10^{-3}	2.2180×10^4	2.3157×10^3
	10	8.0406×10^{-3}	4.8823×10^{-2}	5.2745×10^{-3}	2.6277×10^{-2}	1.8655×10^{-3}	3.8691×10^2	2.3157×10^3
2^{16}	0	2.3512×10^{-5}	1.4404×10^{-4}	1.5128×10^{-5}	7.7041×10^{-5}	5.4111×10^{-6}	7.5550×10^6	–
	8	2.3512×10^{-5}	1.4404×10^{-4}	1.5128×10^{-5}	7.7041×10^{-5}	5.4111×10^{-6}	1.6595×10^3	2.3157×10^3
	11	2.3512×10^{-5}	1.4404×10^{-4}	1.5128×10^{-5}	7.7041×10^{-5}	5.4111×10^{-6}	1.3220×10^2	2.3157×10^3
2^{17}	0	8.5834×10^{-8}	5.2706×10^{-7}	5.4953×10^{-8}	2.8187×10^{-7}	1.9729×10^{-8}	2.8670×10^7	–
	9	8.5834×10^{-8}	5.2705×10^{-7}	5.4953×10^{-8}	2.8187×10^{-7}	1.9729×10^{-8}	1.1834×10^4	2.3157×10^3
	12	8.5834×10^{-8}	5.2706×10^{-7}	5.4953×10^{-8}	2.8187×10^{-7}	1.9729×10^{-8}	3.6510×10^1	2.3157×10^3
2^{18}	0	3.2902×10^{-10}	2.0239×10^{-9}	3.4066×10^{-10}	1.1069×10^{-9}	2.1447×10^{-10}	1.1351×10^8	–
	10	9.3775×10^{-10}	2.0278×10^{-9}	8.9007×10^{-10}	1.1667×10^{-9}	3.9906×10^{-10}	1.0867×10^4	2.3157×10^3
	13	3.2825×10^{-10}	2.0194×10^{-9}	3.3655×10^{-10}	1.0974×10^{-9}	1.3643×10^{-10}	4.2752×10^1	2.3157×10^3

TABLE 2. Relative errors for Example 2 with accuracy order $M = 6$ and $M = 8$. We take $N_0 = 32$ and $s = 1$ in Algorithm 1. The grid increment used in each sub-interval $[(k-1)2^{-3}, k2^{-3}]$ with $1 \leq k \leq 2^3$ is N^{-1} . The largest matrix size of linking problems is 31×31 , which occurs in (S3) of Algorithm 1. The remaining linking problems are solved by 3×3 matrices. Since the analytic solution u_e of this example is known, $\|u_e\|_\infty$, $\|u'_e\|_\infty$, $\|u_e\|_2$, $\|u'_e\|_2$, and $\|u_e\|$ are computed with high precision symbolically.

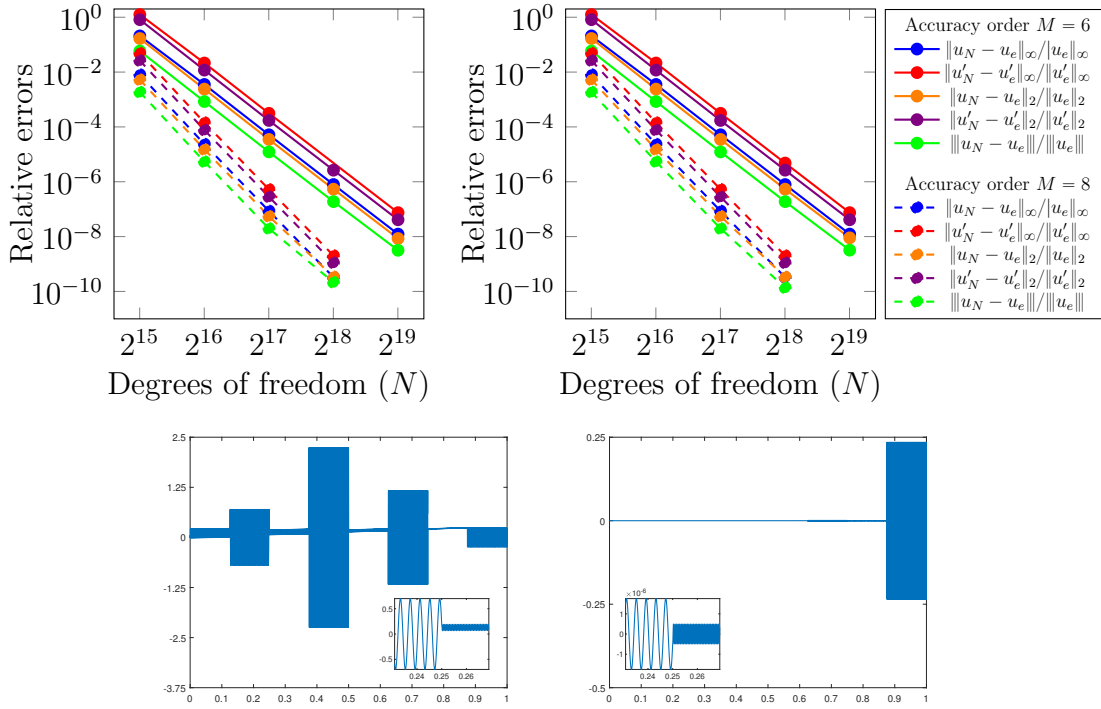


FIGURE 2. Top: The convergence plots for Example 2 without DAT (left) and with DAT (right). The vertical axis uses a base-10 log scale, while the horizontal axis uses a base-2 log scale. Bottom: The real (left) and imaginary (right) parts of the approximated solution of Example 2 obtained from DAT with $N = 2^{19}$ and $\ell = 14$.

Example 3. Consider $[a(x)u'(x)]' + \kappa^2(x)u(x) = f(x)$, $x \in (0, 1)$ with the following coefficients

$$\begin{aligned}
 a &= e^{-x} \chi_{[0, \frac{31}{10}] \cup [\frac{69}{100}, \frac{81}{100}]} + (e^x + 1) \chi_{[\frac{31}{10}, \frac{69}{100}] \cup [\frac{81}{100}, 1]}, \\
 \kappa &= 10^4 e^{2x} \chi_{[0, \frac{31}{10}]} + 10^5 x^4 \chi_{[\frac{31}{10}, \frac{69}{100}]} + 10^4 (1 + x^4) \chi_{[\frac{69}{100}, \frac{81}{100}]} + 10^5 e^{-3x} \chi_{[\frac{81}{100}, 1]}, \\
 f &= 10^7 \left(\chi_{[0, \frac{31}{10}]} + x^2 \chi_{[\frac{31}{10}, \frac{69}{100}]} + x^3 \chi_{[\frac{69}{100}, \frac{81}{100}]} + x^5 \chi_{[\frac{81}{100}, 1]} \right),
 \end{aligned}$$

and the boundary conditions $u(0) = 1$ and $(e + 1)^{1/2} u'(1) - i 10^5 e^{-3} u(1) = 0$. This example shows how DAT is stable with respect to splits and tree levels. For simplicity, we consider a tree level that is not high. Hence, it is to be expected that the maximum condition numbers of the local and linking problems are still relatively large, but are nonetheless smaller than the condition numbers of FDM. In fact, if we look at these condition numbers in granular detail, a large proportion of them are significantly smaller than those of FDM for any given N . See Table 3 for the numerical summary as well as Figures 3 for the convergence and approximation solution plots.

N	(ℓ, s)	$\frac{\ u_{2N} - u_N\ _\infty}{\ u_{2N}\ _\infty}$	$\frac{\ u'_{2N} - u'_N\ _\infty}{\ u'_{2N}\ _\infty}$	$\frac{\ u_{2N} - u_N\ _{L_2}}{\ u_{2N}\ _{L_2}}$	$\frac{\ u'_{2N} - u'_N\ _{L_2}}{\ u'_{2N}\ _{L_2}}$	$\frac{\ u_{2N} - u_N\ }{\ u_{2N}\ }$	Local CN	Link CN
Accuracy order $M = 6$								
2^{15}	(0, 0)	4.7473×10^{-2}	6.7611×10^{-2}	5.2967×10^{-2}	5.9990×10^{-2}	5.8284×10^{-2}	5.1868×10^6	—
	(5, 1)	4.7473×10^{-2}	6.7611×10^{-2}	5.2967×10^{-2}	5.9990×10^{-2}	5.8284×10^{-2}	2.0710×10^5	8.4131×10^3
	(3, 2)	4.7473×10^{-2}	6.7611×10^{-2}	5.2967×10^{-2}	5.9990×10^{-2}	5.8284×10^{-2}	2.0710×10^5	2.8994×10^4
2^{16}	(0, 0)	7.2618×10^{-4}	1.0353×10^{-3}	8.0995×10^{-4}	9.1711×10^{-4}	8.9104×10^{-4}	2.2200×10^7	—
	(5, 1)	7.2618×10^{-4}	1.0353×10^{-3}	8.0995×10^{-4}	9.1711×10^{-4}	8.9103×10^{-4}	8.2933×10^5	8.4131×10^3
	(3, 2)	7.2618×10^{-4}	1.0353×10^{-3}	8.0995×10^{-4}	9.1711×10^{-4}	8.9104×10^{-4}	8.2933×10^5	2.9212×10^4
2^{17}	(0, 0)	1.1182×10^{-5}	1.5959×10^{-5}	1.2472×10^{-5}	1.4123×10^{-5}	1.3722×10^{-5}	8.8893×10^7	—
	(5, 1)	1.1188×10^{-5}	1.5967×10^{-5}	1.2479×10^{-5}	1.4131×10^{-5}	1.3729×10^{-5}	3.3176×10^6	8.4131×10^3
	(3, 2)	1.1179×10^{-5}	1.5958×10^{-5}	1.2469×10^{-5}	1.4119×10^{-5}	1.3718×10^{-5}	3.3176×10^6	2.9215×10^4
2^{18}	(0, 0)	1.7281×10^{-7}	2.4671×10^{-7}	1.9273×10^{-7}	2.1820×10^{-7}	2.1200×10^{-7}	3.5557×10^8	—
	(5, 1)	1.6145×10^{-7}	2.3070×10^{-7}	1.7999×10^{-7}	2.0357×10^{-7}	1.9773×10^{-7}	1.3271×10^7	8.4131×10^3

	(3, 2)	1.7927×10^{-7}	2.5563×10^{-7}	1.9995×10^{-7}	2.2636×10^{-7}	2.1996×10^{-7}	1.3271×10^7	2.9215×10^4
Accuracy order $M = 8$								
2^{15}	(0, 0)	2.4465×10^{-4}	3.3087×10^{-4}	2.7084×10^{-4}	2.9990×10^{-4}	2.9367×10^{-4}	5.5576×10^6	—
	(5, 1)	2.4465×10^{-4}	3.3087×10^{-4}	2.7084×10^{-4}	2.9990×10^{-4}	2.9367×10^{-4}	2.0710×10^5	8.4131×10^3
	(3, 2)	2.4465×10^{-4}	3.3087×10^{-4}	2.7084×10^{-4}	2.9990×10^{-4}	2.9367×10^{-4}	2.0710×10^5	2.9216×10^4
2^{16}	(0, 0)	8.7748×10^{-7}	1.1834×10^{-6}	9.7051×10^{-7}	1.0726×10^{-6}	1.0509×10^{-6}	2.2223×10^7	—
	(5, 1)	8.8029×10^{-7}	1.1867×10^{-6}	9.7356×10^{-7}	1.0758×10^{-6}	1.0542×10^{-6}	8.2933×10^5	8.4131×10^3
	(3, 2)	8.7595×10^{-7}	1.1813×10^{-6}	9.6881×10^{-7}	1.0707×10^{-6}	1.0491×10^{-6}	8.2933×10^5	2.9215×10^4
2^{17}	(0, 0)	3.7755×10^{-9}	5.0250×10^{-9}	4.1685×10^{-9}	4.5953×10^{-9}	4.5071×10^{-9}	8.8894×10^7	—
	(5, 1)	3.2508×10^{-9}	6.3200×10^{-9}	3.9897×10^{-9}	5.2716×10^{-9}	5.0029×10^{-9}	3.3176×10^6	8.4131×10^3
	(3, 2)	6.9405×10^{-9}	9.3269×10^{-9}	7.6890×10^{-9}	8.5585×10^{-9}	8.3687×10^{-9}	3.3176×10^6	2.9215×10^4

TABLE 3. Relative errors for Example 3 with accuracy order $M = 6$ and $M = 8$. We take $N_0 = 32$ and $s \in \{1, 2\}$ in Algorithm 1. The grid increments used in $[0, \frac{31}{100}]$, $[\frac{31}{100}, \frac{69}{100}]$, $[\frac{69}{100}, \frac{81}{100}]$, and $[\frac{81}{100}, 1]$ are respectively $\frac{31}{100N}$, $\frac{19}{50N}$, $\frac{3}{25N}$, and $\frac{19}{100N}$. The largest matrix size of linking problems for $s = 1, 2$ is 31×31 , which occurs in (S3) of Algorithm 1. The remaining linking problems are solved by 3×3 matrices for $s = 1$ and 7×7 matrices for $s = 2$.

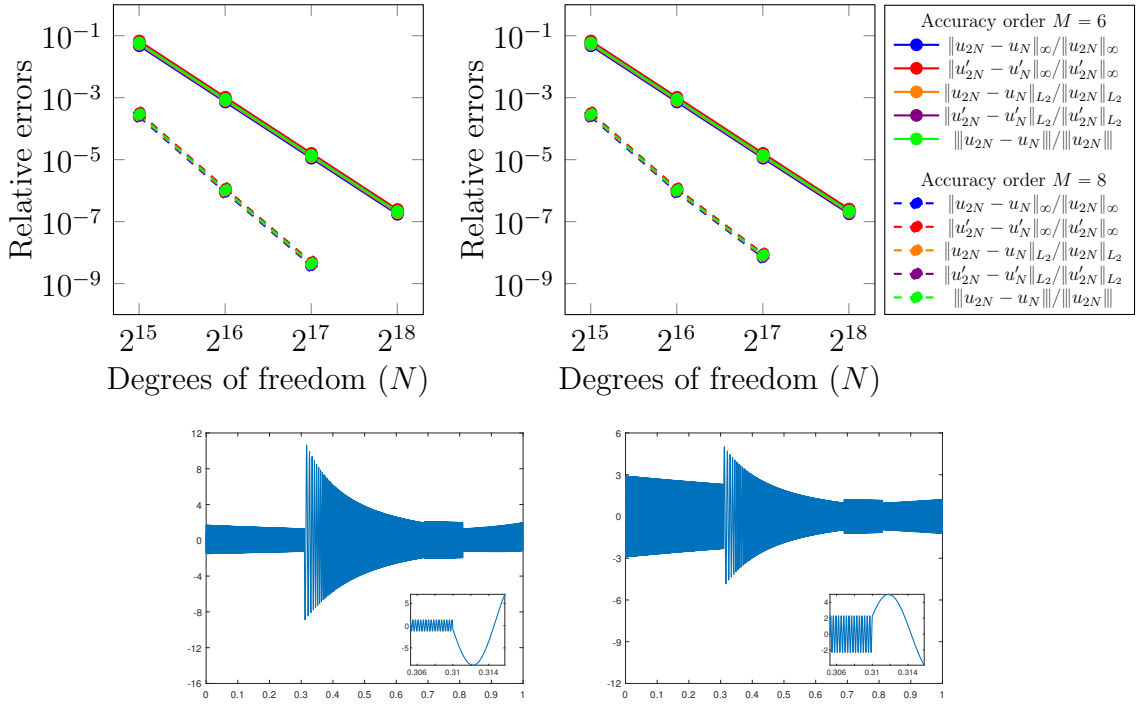


FIGURE 3. Top: The convergence plots for Example 3 without DAT (left) and with DAT (right). The vertical axis uses a base-10 log scale, while the horizontal axis uses a base-2 log scale. Bottom: The real (left) and imaginary (right) parts of the approximated solution of Example 3 obtained from DAT with $N = 2^{18} + 1$ and $(\ell, s) = (5, 1)$.

Example 4. Consider $[a(x)u'(x)]' + \kappa^2(x)u(x) = f(x)$, $x \in (0, 1)$ with the following coefficients

$$a = 1.1 + \sin(40\pi x), \quad \kappa = 10^5 (1 - (x - 0.5)^2), \quad f = 10^9(x^7 + 1),$$

and the boundary conditions $\sqrt{1.1}u'(0) + i75000u(0) = -1$ and $\sqrt{1.1}u'(1) - i75000u(1) = 0$. The analytic expression of the exact solution is unknown. See Table 4 for the numerical summary as well as Figure 4 for the convergence and approximated solution plots.

N	ℓ	$\frac{\ u_{2N-1}-u_N\ _\infty}{\ u_{2N-1}\ _\infty}$	$\frac{\ u'_{2N-1}-u'_N\ _\infty}{\ u'_{2N-1}\ _\infty}$	$\frac{\ u_{2N-1}-u_N\ _2}{\ u_{2N-1}\ _2}$	$\frac{\ u'_{2N-1}-u'_N\ _{L_2}}{\ u'_{2N-1}\ _{L_2}}$	$\frac{\ u_{2N-1}-u_N\ }{\ u_{2N-1}\ }$	Local CN	Link CN
Accuracy order $M = 6$								
$2^{18} + 1$	0	4.8707×10^{-1}	7.6812×10^{-1}	6.3898×10^{-1}	7.6976×10^{-1}	6.9749×10^{-1}	5.5287×10^6	—
	16	4.8707×10^{-1}	7.6812×10^{-1}	6.3898×10^{-1}	7.6976×10^{-1}	6.9754×10^{-1}	2.7421×10^5	7.7100×10^6
$2^{19} + 1$	0	7.1208×10^{-3}	1.1068×10^{-2}	9.1539×10^{-3}	1.0998×10^{-2}	9.9643×10^{-3}	1.4748×10^7	—
	17	7.1208×10^{-3}	1.1068×10^{-2}	9.1539×10^{-3}	1.0998×10^{-2}	9.9643×10^{-3}	4.3855×10^1	1.1590×10^7
$2^{20} + 1$	0	1.0754×10^{-4}	1.6712×10^{-4}	1.3822×10^{-4}	1.6607×10^{-4}	1.5046×10^{-4}	6.2128×10^7	—
	18	1.0754×10^{-4}	1.6712×10^{-4}	1.3822×10^{-4}	1.6607×10^{-4}	1.5046×10^{-4}	4.4716×10^1	1.1877×10^7
$2^{21} + 1$	0	1.6652×10^{-6}	2.5876×10^{-6}	2.1401×10^{-6}	2.5713×10^{-6}	2.3295×10^{-6}	2.2335×10^8	—
	19	1.6652×10^{-6}	2.5877×10^{-6}	2.1402×10^{-6}	2.5714×10^{-6}	2.3296×10^{-6}	4.4931×10^1	1.1882×10^7
$2^{22} + 1$	0	1.9579×10^{-8}	3.1304×10^{-8}	2.5739×10^{-8}	3.0895×10^{-8}	2.8018×10^{-8}	9.2078×10^8	—
	20	1.9862×10^{-8}	3.1727×10^{-8}	2.6078×10^{-8}	3.1301×10^{-8}	2.8386×10^{-8}	4.4984×10^1	1.1882×10^7
Accuracy order $M = 8$								
$2^{18} + 1$	0	6.7606×10^{-3}	1.0602×10^{-2}	8.7825×10^{-3}	1.0559×10^{-2}	9.5649×10^{-3}	5.6623×10^6	—
	16	6.7606×10^{-3}	1.0602×10^{-2}	8.7825×10^{-3}	1.0559×10^{-2}	9.5649×10^{-3}	5.2518×10^5	1.2023×10^7
$2^{19} + 1$	0	2.2709×10^{-5}	3.5577×10^{-5}	2.9456×10^{-5}	3.5414×10^{-5}	3.2078×10^{-5}	1.4237×10^7	—
	17	2.2709×10^{-5}	3.5577×10^{-5}	2.9456×10^{-5}	3.5414×10^{-5}	3.2078×10^{-5}	4.3855×10^1	1.1882×10^7
$2^{20} + 1$	0	8.6824×10^{-8}	1.3591×10^{-7}	1.1250×10^{-7}	1.3525×10^{-7}	1.2250×10^{-7}	5.9762×10^7	—
	18	8.6814×10^{-8}	1.3589×10^{-7}	1.1248×10^{-7}	1.3525×10^{-7}	1.2249×10^{-7}	4.4716×10^1	1.1882×10^7
$2^{21} + 1$	0	1.9291×10^{-9}	2.9177×10^{-9}	2.3844×10^{-9}	2.8620×10^{-9}	2.5935×10^{-9}	2.2250×10^8	—
	19	1.8549×10^{-9}	2.8085×10^{-9}	2.2962×10^{-9}	2.7567×10^{-9}	2.4979×10^{-9}	4.4931×10^1	1.1882×10^7

TABLE 4. Relative errors for Example 4 with accuracy order $M = 6$ and $M = 8$. We take $N_0 = 4$ and $s = 1$ in Algorithm 1. The grid increment used in $[0, 1]$ is $(N - 1)^{-1}$. All linking problems are solved by 3×3 matrices.

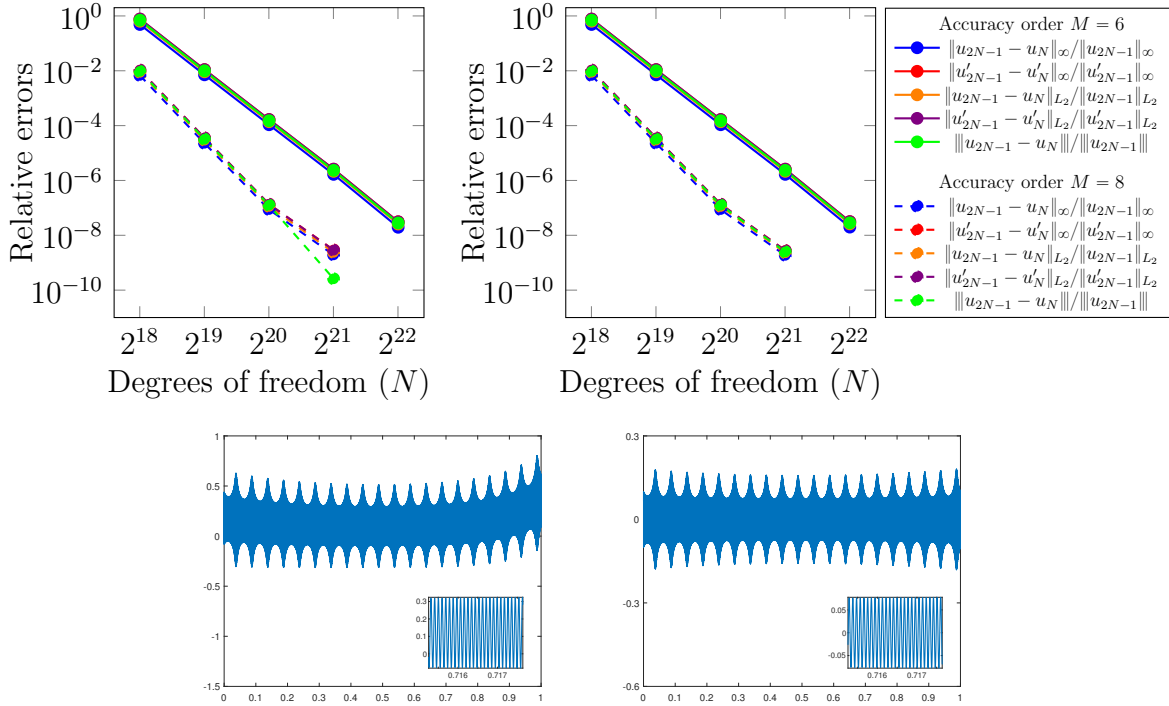


FIGURE 4. Top: The convergence plots for Example 4 without DAT (left) and with DAT (right). The vertical axis uses a base-10 log scale, while the horizontal axis uses a base-2 log scale. Bottom: The real (left) and imaginary (right) parts of the approximated solution of Example 4 obtained from DAT with $N = 2^{22} + 1$ and $\ell = 20$.

Example 5. Consider $[a(x)u'(x)]' + \kappa^2(x)u(x) = f(x)$, $x \in (0, 1)$ with the following coefficients

$$a = (5 + \sin(10\pi x))\chi_{[0, \frac{23}{100}] \cup [\frac{83}{100}, 1]} + (2 + \sin(10\pi x))\chi_{[\frac{23}{100}, \frac{53}{100}]} + (9 + \sin(10\pi x))\chi_{[\frac{53}{100}, \frac{83}{100}]},$$

$$\kappa = i \left(100x^3\chi_{[0, \frac{23}{100}]} + 10\chi_{[\frac{23}{100}, \frac{53}{100}]} + 20e^x\chi_{[\frac{53}{100}, \frac{83}{100}]} + 40\chi_{[\frac{83}{100}, 1]} \right),$$

$$f = 2^8 \left(\cosh(x)\chi_{[0, \frac{23}{100}]} + \sinh(x)\chi_{[\frac{23}{100}, \frac{53}{100}]} - \cosh(x)\chi_{[\frac{53}{100}, \frac{83}{100}]} - \sinh(x)\chi_{[\frac{83}{100}, 1]} \right),$$

and the boundary conditions $u(0) = 1$ and $u(1) = 0$. See Table 5 for the numerical summary as well as Figure 5 for the convergence plots.

N	ℓ	$\frac{\ u_{2N+1} - u_N\ _\infty}{\ u_{2N+1}\ _\infty}$	$\frac{\ u'_{2N+1} - u'_N\ _\infty}{\ u'_{2N+1}\ _\infty}$	$\frac{\ u_{2N+1} - u_N\ _{L_2}}{\ u_{2N+1}\ _{L_2}}$	$\frac{\ u'_{2N+1} - u'_N\ _{L_2}}{\ u'_{2N+1}\ _{L_2}}$	$\frac{\ u_{2N+1} - u_N\ }{\ u_{2N+1}\ }$	Local CN	Link CN
Accuracy order $M = 6$								
$2^5 - 1$	0	1.6165×10^{-3}	5.1562×10^{-3}	1.7685×10^{-3}	3.6918×10^{-3}	1.9581×10^{-3}	1.4917×10^2	—
	1	1.6165×10^{-3}	5.1562×10^{-3}	1.7685×10^{-3}	3.6918×10^{-3}	1.9581×10^{-3}	1.1301×10^1	2.3689×10^1
$2^6 - 1$	0	1.9225×10^{-5}	1.0085×10^{-4}	1.6868×10^{-5}	6.7101×10^{-5}	3.5531×10^{-5}	6.7855×10^2	—
	2	1.9225×10^{-5}	1.0085×10^{-4}	1.6868×10^{-5}	6.7101×10^{-5}	3.5531×10^{-5}	8.8132	2.3655×10^1
$2^7 - 1$	0	2.9984×10^{-7}	1.3933×10^{-6}	2.4917×10^{-7}	7.5088×10^{-7}	4.6062×10^{-7}	2.8801×10^3	—
	3	2.9984×10^{-7}	1.3933×10^{-6}	2.4917×10^{-7}	7.5088×10^{-7}	4.6062×10^{-7}	8.4129	2.3655×10^1
$2^8 - 1$	0	4.6292×10^{-9}	2.1237×10^{-8}	3.7625×10^{-9}	1.1588×10^{-8}	7.1264×10^{-9}	1.1776×10^4	—
	4	4.6291×10^{-9}	2.1237×10^{-8}	3.7625×10^{-9}	1.1588×10^{-8}	7.1264×10^{-9}	8.7543	2.3655×10^1
$2^9 - 1$	0	7.2079×10^{-11}	3.3915×10^{-10}	5.8223×10^{-11}	1.8448×10^{-10}	1.1245×10^{-10}	4.7524×10^4	—
	5	7.1794×10^{-11}	3.3986×10^{-10}	5.7435×10^{-11}	1.8453×10^{-10}	1.1222×10^{-10}	8.8858	2.3655×10^1
Accuracy order $M = 8$								
$2^5 - 1$	0	4.5909×10^{-4}	3.2074×10^{-3}	4.5427×10^{-4}	2.2250×10^{-3}	1.0600×10^{-3}	1.4872×10^3	—
	1	4.5909×10^{-4}	3.2074×10^{-3}	4.5427×10^{-4}	2.2250×10^{-3}	1.0600×10^{-3}	1.1303×10^1	2.3630×10^1
$2^6 - 1$	0	1.6230×10^{-6}	1.7559×10^{-5}	1.2563×10^{-6}	1.0149×10^{-5}	4.3083×10^{-6}	6.7856×10^2	—
	2	1.6230×10^{-6}	1.7559×10^{-5}	1.2563×10^{-6}	1.0149×10^{-5}	4.3083×10^{-6}	8.8132	2.3655×10^1
$2^7 - 1$	0	2.6892×10^{-9}	5.4167×10^{-8}	1.5333×10^{-9}	2.8388×10^{-8}	1.2377×10^{-8}	2.8801×10^3	—
	3	2.6892×10^{-9}	5.4167×10^{-8}	1.5334×10^{-9}	2.8388×10^{-8}	1.2377×10^{-8}	8.4129	2.3655×10^1
$2^8 - 1$	0	9.2581×10^{-12}	2.2481×10^{-10}	5.3351×10^{-12}	1.1073×10^{-10}	4.8411×10^{-11}	1.1776×10^4	—
	4	9.2223×10^{-12}	2.2484×10^{-10}	5.2987×10^{-12}	1.1075×10^{-10}	4.8417×10^{-11}	8.7543	2.3655×10^1

TABLE 5. Relative errors for Example 5 with accuracy order $M = 6$ and $M = 8$. We take $N_0 = 16$ and $s = 1$ in Algorithm 1. The grid increments used in $[0, \frac{23}{100}]$, $[\frac{23}{100}, \frac{53}{100}]$, $[\frac{53}{100}, \frac{83}{100}]$, and $[\frac{83}{100}, 1]$ are respectively $\frac{23}{400(N+1)}$, $\frac{3}{40(N+1)}$, $\frac{3}{40(N+1)}$, and $\frac{17}{400(N+1)}$. The largest matrix size of linking problems is 15×15 , which occurs in (S3) of Algorithm 1.

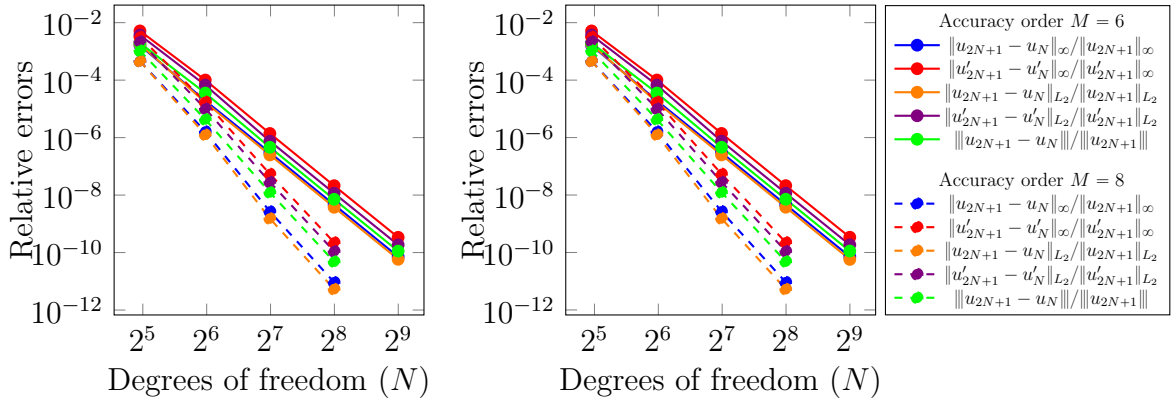


FIGURE 5. The convergence plots for Example 5 without DAT (left) and with DAT (right). The vertical axis uses a base-10 log scale, while the horizontal axis uses a base-2 log scale.

4.2. Numerical experiments on 2D Helmholtz equations. Note that separable 2D Helmholtz equations can be converted into a sequence of 1D Helmholtz problems (e.g, see [28, 29]), to which we may apply DAT as demonstrated below.

Example 6. Let $D_1 := \{(r, \theta) : 1 \leq r < 2, \theta \in [0, 2\pi)\}$, $D_2 := \{(r, \theta) : 2 \leq r \leq 4, \theta \in [0, 2\pi)\}$, and $D := D_1 \cup D_2$. Consider the following 2D Helmholtz equation $\nabla \cdot (\nabla u) + \kappa^2 u = 0$ on the domain D , which can be rewritten in polar coordinates as follows:

$$\begin{aligned} \frac{1}{r} \frac{\partial}{\partial r} \left(r \frac{\partial u}{\partial r} \right) + \frac{1}{r^2} \frac{\partial^2 u}{\partial \theta^2} + \kappa^2 u &= 0 \quad \text{on } D, \\ \frac{\partial u}{\partial r} \Big|_{r=1} &= 0, \quad \left(\frac{\partial u}{\partial r} + \left(\frac{1}{2r} - 100i \right) u \right) \Big|_{r=4} = \left(\frac{\partial u_I}{\partial r} + \left(\frac{1}{2r} - 100i \right) u_I \right) \Big|_{r=4}, \end{aligned}$$

where $\kappa = 50\chi_{D_1} + 100\chi_{D_2}$ and $u_I := \sum_{m=0}^{\infty} i^m (\chi_{(m=0)} + 2\chi_{(m>0)}) J_m(100r) \cos(m\theta)$. To derive the analytic reference solution, u_e , we can use the method outlined in [16, Section 7.1]. By separation of variables (i.e, let $\partial^2 u / \partial \theta^2 = -m^2$ and $u = r^{-1/2} v$), we obtain the following 1D Helmholtz equations

$$\begin{aligned} v_m'' + \left(50^2 \chi_{[1,2)} + 100^2 \chi_{[2,4]} - \frac{1}{r^2} \left(m^2 - \frac{1}{4} \right) \right) v_m &= 0, \quad r \in (1, 4), \quad m \in \mathbb{N}_0 \\ \left(v_m' - \frac{1}{2} v_m \right) \Big|_{r=1} &= 0, \\ (v_m' - 100i v_m) \Big|_{r=4} &= 2i^m (\chi_{(m=0)} + 2\chi_{(m>0)}) \left(100 J_m'(400) + \left(\frac{1}{8} - 100i \right) J_m(400) \right). \end{aligned} \tag{4.3}$$

Our approximated solution is of the form $u_N = \sum_{m=0}^{641} r^{-1/2} v_{m,N} \cos(m\theta)$, where $v_{m,N}$ is the approximated solution to v_m in (4.3) using N points. In all cases, we use 2049 points to discretize the angle θ in our exact and approximated solutions. Also note that the following ‘‘Local CN’’ and ‘‘Link CN’’ record the maximum condition number of all local problems and all $m = 1, \dots, 641$.

N	ℓ	$\frac{\ u_N - u_e\ _{\infty}}{\ u_e\ _{\infty}}$	$\frac{\ u_N - u_e\ _{L_2}}{\ u_e\ _{L_2}}$	Local CN	Link CN
Accuracy order $M = 6$					
$2^8 + 1$	0	1.0461×10^{-1}	6.6021×10^{-2}	1.8359×10^5	–
	5	1.0461×10^{-1}	6.6021×10^{-2}	4.7907×10^4	3.0499×10^5
$2^9 + 1$	0	1.2885×10^{-3}	7.6950×10^{-4}	4.0426×10^4	–
	6	1.2885×10^{-3}	7.6950×10^{-4}	7.0618×10^2	2.7844×10^5
$2^{10} + 1$	0	1.9204×10^{-5}	1.1290×10^{-5}	1.5220×10^5	–
	7	1.9204×10^{-5}	1.1290×10^{-5}	4.7774×10^1	2.7808×10^5
$2^{11} + 1$	0	2.9671×10^{-7}	1.7375×10^{-7}	6.0129×10^5	–
	8	2.9671×10^{-7}	1.7375×10^{-7}	4.5620×10^1	2.7807×10^5
$2^{12} + 1$	0	4.6285×10^{-9}	2.7076×10^{-9}	2.3977×10^6	–
	9	4.6295×10^{-9}	2.7082×10^{-9}	4.5133×10^1	2.7807×10^5
Accuracy order $M = 8$					
$2^8 + 1$	0	6.8220×10^{-3}	3.4958×10^{-3}	1.7918×10^5	–
	5	6.8220×10^{-3}	3.4958×10^{-3}	9.1254×10^4	2.8071×10^5
$2^9 + 1$	0	2.7208×10^{-5}	1.4102×10^{-5}	4.0445×10^4	–
	6	2.7208×10^{-5}	1.4102×10^{-5}	7.0535×10^2	2.7807×10^5
$2^{10} + 1$	0	1.0825×10^{-7}	5.5999×10^{-8}	1.5220×10^5	–
	7	1.0825×10^{-7}	5.5999×10^{-8}	4.7774×10^1	2.7807×10^5
$2^{11} + 1$	0	4.2441×10^{-10}	2.1932×10^{-10}	6.0129×10^5	–
	8	4.2435×10^{-10}	2.1934×10^{-10}	4.5620×10^1	2.7807×10^5

TABLE 6. Relative errors for Example 6 with accuracy order $M = 6$ and $M = 8$. We take $N_0 = 8$ and $s = 1$ in Algorithm 1. The grid increments used in each $[1, 2]$ and $[2, 4]$ are respectively $(2N - 2)^{-1}$ and $(N - 1)^{-1}$. The largest matrix size of linking problems is 7×7 , which occurs in (S3) of Algorithm 1. The remaining linking problems are solved by 3×3 matrices.

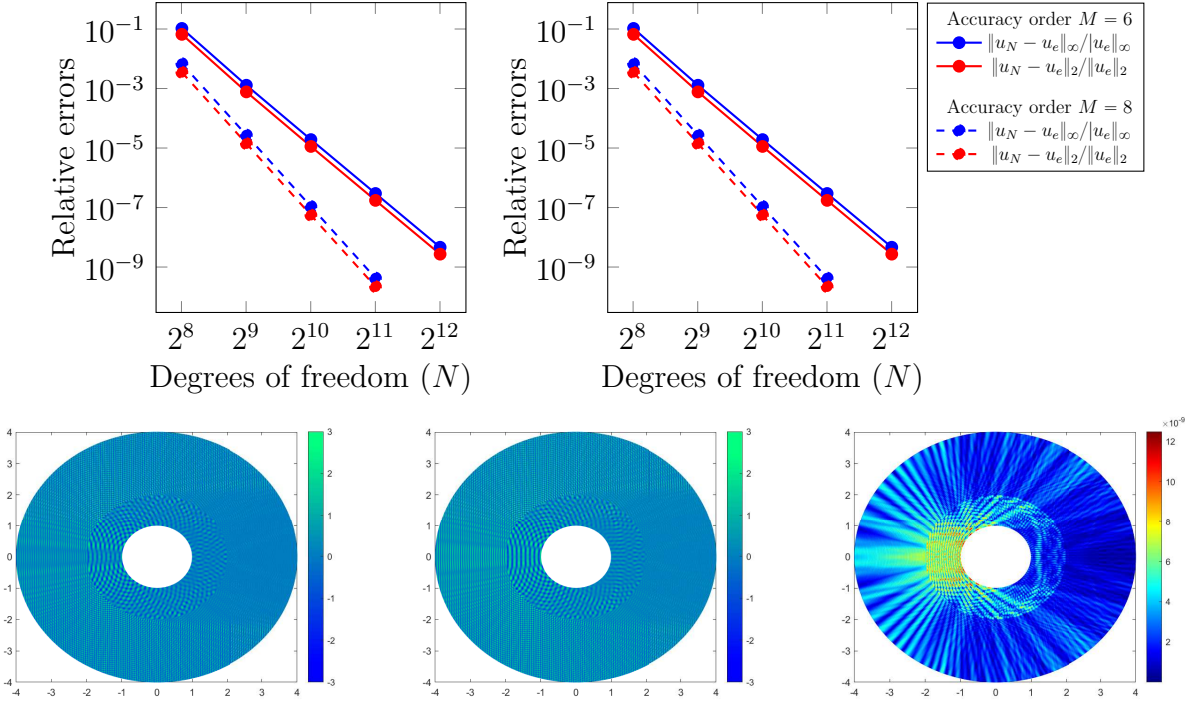


FIGURE 6. Top: The convergence plots for Example 6 without DAT (left) and with DAT (right). The vertical axis uses a base-10 log scale, while the horizontal axis uses a base-2 log scale. Bottom: The real (left) and imaginary (middle) parts of the approximated solution of Example 6 obtained from DAT with $N = 2^{12} + 1$ and $\ell = 9$ as well as the error of the approximated solution (right) of Example 6 obtained from DAT with $N = 2^{12} + 1$ and $\ell = 9$.

4.3. DAT and compact finite difference methods using only function values. The direct usage of derivatives of a, κ^2, f in Theorems 3.2 and 3.3 may not be computationally efficient. These derivatives can in fact be estimated by using only function values of a, κ^2, f through local polynomial approximation. For example, if we consider an interior stencil of the form (3.11) and (3.12), we know from (3.1) that all stencil coefficients depend on $a(x_b), a'(x_b), \dots, a^{(M)}(x_b), \kappa^2(x_b), [\kappa^2]'(x_b), \dots, [\kappa^2]^{(M-2)}(x_b)$, and $f(x_b), f'(x_b), \dots, f^{(M-2)}(x_b)$. For the sake of illustration, consider $a(x_b), a'(x_b), \dots, a^{(M)}(x_b)$. Let $J \geq M$ and take $J + 1$ points $\{x_j\}_{j=0}^J$ near the base point x_b such that all the points fall into one piece of the piecewise smooth functions a, κ^2 and f . Find the unique polynomial p of degree J satisfying $p(x_j) = a(x_j)$ for all $j = 0, \dots, J$. Then $a^{(j)}(x_b) \approx p^{(j)}(x_b)$ for $j = 0, \dots, M$. For simplicity, we often require $x_b \in \{x_j\}_{j=0}^J$ and take $J = M$ and $\{x_j\}_{j=0}^J$ to be evenly spaced with mesh size $h/2$.

Using only function values without explicitly using the true derivatives, we re-calculate numerical experiments in Examples 1–6. The numerical performance in all examples is very much comparable and almost the same as those using derivatives explicitly. To illustrate the performance of our proposed methods using only function values with derivatives, here for simplicity of presentation, we only provide one example below for re-calculating Example 3 by only using function values.

N	(ℓ, s)	$\frac{\ u_{2N}-u_N\ _\infty}{\ u_{2N}\ _\infty}$	$\frac{\ u'_{2N}-u'_N\ _\infty}{\ u'_{2N}\ _\infty}$	$\frac{\ u_{2N}-u_N\ _{L_2}}{\ u_{2N}\ _{L_2}}$	$\frac{\ u'_{2N}-u'_N\ _{L_2}}{\ u'_{2N}\ _{L_2}}$	$\frac{\ u_{2N}-u_N\ }{\ u_{2N}\ }$	Local CN	Link CN
Accuracy order $M = 6$								
2^{15}	(0, 0)	4.7473×10^{-2}	6.7611×10^{-2}	5.2967×10^{-2}	5.9990×10^{-2}	5.8284×10^{-2}	5.1868×10^6	—
	(5, 1)	4.7473×10^{-2}	6.7611×10^{-2}	5.2967×10^{-2}	5.9990×10^{-2}	5.8284×10^{-2}	2.0710×10^5	8.4131×10^3
	(3, 2)	4.7473×10^{-2}	6.7611×10^{-2}	5.2967×10^{-2}	5.9990×10^{-2}	5.8284×10^{-2}	2.0710×10^5	2.8994×10^4
	(2, 4)	4.7473×10^{-2}	6.7611×10^{-2}	5.2967×10^{-2}	5.9990×10^{-2}	5.8284×10^{-2}	2.0710×10^5	8.1385×10^4
2^{16}	(0, 0)	7.2618×10^{-4}	1.0353×10^{-3}	8.0995×10^{-4}	9.1711×10^{-4}	8.9104×10^{-4}	2.2200×10^7	—
	(5, 1)	7.2618×10^{-4}	1.0353×10^{-3}	8.0995×10^{-4}	9.1711×10^{-4}	8.9103×10^{-4}	8.2933×10^5	8.4131×10^3
	(3, 2)	7.2618×10^{-4}	1.0353×10^{-3}	8.0995×10^{-4}	9.1711×10^{-4}	8.9104×10^{-4}	8.2933×10^5	2.9212×10^4
	(2, 4)	7.2618×10^{-4}	1.0353×10^{-3}	8.0995×10^{-4}	9.1711×10^{-4}	8.9104×10^{-4}	8.2933×10^5	8.1511×10^4
2^{17}	(0, 0)	1.1182×10^{-5}	1.5959×10^{-5}	1.2472×10^{-5}	1.4123×10^{-5}	1.3722×10^{-5}	8.8893×10^7	—
	(5, 1)	1.1188×10^{-5}	1.5967×10^{-5}	1.2479×10^{-5}	1.4131×10^{-5}	1.3729×10^{-5}	3.3176×10^6	8.4131×10^3
	(3, 2)	1.1179×10^{-5}	1.5955×10^{-5}	1.2469×10^{-5}	1.4119×10^{-5}	1.3718×10^{-5}	3.3176×10^6	2.9215×10^4
	(2, 4)	1.1182×10^{-5}	1.5958×10^{-5}	1.2472×10^{-5}	1.4123×10^{-5}	1.3721×10^{-5}	3.3176×10^6	8.1513×10^4
2^{18}	(0, 0)	1.7274×10^{-7}	2.4663×10^{-7}	1.9265×10^{-7}	2.1812×10^{-7}	2.1192×10^{-7}	3.5557×10^8	—
	(5, 1)	1.6132×10^{-7}	2.3056×10^{-7}	1.7986×10^{-7}	2.0343×10^{-7}	1.9759×10^{-7}	1.3271×10^7	8.4131×10^3
	(3, 2)	1.7914×10^{-7}	2.5548×10^{-7}	1.9981×10^{-7}	2.2622×10^{-7}	2.1981×10^{-7}	1.3271×10^7	2.9215×10^4
	(2, 4)	1.7312×10^{-7}	2.4772×10^{-7}	1.9326×10^{-7}	2.1907×10^{-7}	2.1277×10^{-7}	1.3271×10^7	8.1513×10^4

TABLE 7. Relative errors for Example 3 using point values with accuracy order $M = 6$.

REFERENCES

- [1] I. M. Babuska and S. A. Sauter, Is the pollution effect of the FEM avoidable for the Helmholtz equation considering high wave numbers? *SIAM Rev.* **42** (2000), no. 3, 451-484.
- [2] S. Britt, S. Tsynkov, and E. Turkel, Numerical simulation of time-harmonic waves in inhomogeneous media using compact high order schemes. *Commun. Comput. Phys.* **9** (2011), no. 3, 520-541.
- [3] E. Burman, H. Wu, and L. Zhu, Linear continuous interior penalty finite element method for Helmholtz equation with high wave number: one-dimensional analysis. *Numer. Meth. Par. Diff. Equ.* **32** (2016), 1378-1410.
- [4] T. Chaumont-Frelet, On high order methods for the heterogeneous Helmholtz equation. *Comput. Math. with Appl.* **72**, no. 9, 2203-2225.
- [5] Z. Chen, D. Cheng, W. Feng, and T. Wu, An optimal 9-point finite difference scheme for the Helmholtz equation with PML. *Int. J. Numer. Anal. Mod.* **10** (2013), no. 2, 389-410.
- [6] H. Dastour and W. Liao, A fourth-order optimal finite difference scheme for the Helmholtz equation with PML. *Comput. Math. Appl.* **78** (2019), 2147-216.
- [7] O. G. Ernst and M. J. Gander, Why is it difficult to solve Helmholtz problems with classical iterative methods. *Lecture Notes in Computational Science and Engineering*, **83** (2011), 325-363.
- [8] X. Feng and H. Wu, Discontinuous Galerkin methods for the Helmholtz equation with large wave number. *SIAM J. Numer. Anal.* **47** (2009), no. 4, 2872-2896.
- [9] X. Feng, X. Li, and Z. Qiao, High order compact finite difference schemes for the Helmholtz equation with discontinuous coefficients. *J. Comput. Math.* **29** (2011), no. 3, 324-340.
- [10] X. Feng, A high-order compact scheme for the one-dimensional Helmholtz equation with a discontinuous coefficient. *Int. J. Numer. Anal. Mod.* **89** (2012), no. 5, 618-624.
- [11] Y. Fu, Compact fourth-order finite difference schemes for Helmholtz equation with high wave numbers. *J. Comput. Math.* **26** (2008), no. 1, 98-111.
- [12] S. Fu and K. Gao, A fast solver for the Helmholtz equation based on the generalized multiscale finite-element method. *Geophys. J. Int.*, **211** (2017), 797-813.
- [13] M. J. Gander and H. Zhang, A class of iterative solvers for the Helmholtz equation: factorizations, sweeping preconditioners, source transfer, single layer potentials, polarized traces, and optimized Schwarz methods. *SIAM Rev.* **61** (2019), no. 1, 3-76.
- [14] R. Hiptmair, A. Moiola, and I. Perugia, A survey of Trefftz methods for the Helmholtz equation. *Lecture Notes in Computational Science and Engineering*, **114** (2016), 237-279.
- [15] I. G. Graham and S. A. Sauter, Stability and finite element error analysis for the Helmholtz equation with variable coefficients. *Math. Comp.*, **89** (2020), no. 321, 105-138.
- [16] O. Lagrouche, P. Bettess, E. Perrey-Debain, and J. Trevelyan, Wave interpolation finite elements for Helmholtz problems with jumps in the wave speed. *Comput. Methods Appl. Mech. Engrg.* **194** (2005), 367-381.

- [17] J. M. Melenk and I. Babuska, The partition of unity finite element method: basic theory and applications. *Comput. Methods Appl. Mech. Engrg.*, **139** (1996), 289-314.
- [18] J. M. Melenk and S. Sauter, Wavenumber explicit convergence analysis for Galerkin discretizations of the Helmholtz equation. *SIAM J. Numer. Anal.* **49** (2011), no. 3, 1210-1243.
- [19] J. Popovic and Olof Runborg, Analysis of a fast method for solving the high frequency Helmholtz equation in one dimension. *BIT Numer. Math.* **51** (2011), 721-755.
- [20] M. Nabavi, M. H. Kamran Siddiqui, and J. Dargahi, A new 9-point sixth-order accurate compact finite-difference method for the Helmholtz equation. *J. Sound. Vib.* **307** (2007), 972-982.
- [21] S. O. Settle, C. C. Douglas, I. Kim, and D. Sheen, On the derivation of highest-order compact finite difference schemes for the one- and two-dimensional Poisson equation with Dirichlet boundary conditions. *SIAM J. Numer. Anal.* **51** (2013), no. 4, 2470-2490.
- [22] T. W. Sheu, L. W. Hsieh, and C. F. Chen, Development of a three-point sixth-order Helmholtz scheme. *J. Comput. Acoust.* **16** (2008), no. 3, 343-359.
- [23] I. Singer and E. Turkel, High-order finite difference methods for the Helmholtz equation. *Comput. Methods Appl. Mech. Engrg.* **163** (1997), 343-358.
- [24] X. Su, X. Feng, and Z. Li, Fourth-order compact schemes for Helmholtz equations with piecewise wave numbers in the polar coordinates. *J. Comput. Math.* **34** (2016), 499-510.
- [25] E. Turkel, D. Gordon, R. Gordon, and S. Tsynkov, Compact 2D and 3D sixth order schemes for the Helmholtz equation with variable wave number. *J. Comp. Phys.* **232** (2013), 272-287.
- [26] D. Wang, R. Tezaur, J. Toivanen, and C. Farhat, Overview of the discontinuous enrichment method, the ultra-weak variational formulation, and the partition of unity method for acoustic scattering in the medium frequency regime and performance comparisons. *Int. J. Numer. Meth. Engrg.* **89** (2012), 403-417.
- [27] K. Wang and Y. S. Wong, Pollution-free finite difference schemes for non-homogeneous Helmholtz equation. *Int. J. Numer. Anal. Mod.* **11** (2014), no. 4, 787-815.
- [28] K. Wang and Y. S. Wong, Is pollution effect of finite difference schemes avoidable for multi-dimensional Helmholtz equations with high wave numbers? *Commun. Comput. Phys.* **21** (2017), no. 2, 490-514.
- [29] K. Wang, Y. S. Wong, and J. Huang, Solving Helmholtz equation at high wave numbers in exterior domains. *Appl. Math. Comp.* **298** (2017), 221-235.
- [30] T. Wu and R. Xu, An optimal compact sixth-order finite difference scheme for the Helmholtz equation. *Comput. Math. Appl.* **75** (2018), 2520-2537.
- [31] Y. S. Wong and G. Li, Exact finite difference schemes for solving Helmholtz equation at any wave number. *Int. J. Numer. Anal. Mod.* **2** (2011), no. 1, 91-108.
- [32] Y. Zhang, K. Wang, and R. Guo, Sixth-order finite difference scheme for the Helmholtz equation with inhomogeneous Robin boundary condition. *Adv. Differ. Equ.* **362** (2019), 1-15.

DEPARTMENT OF MATHEMATICAL AND STATISTICAL SCIENCES, UNIVERSITY OF ALBERTA, EDMONTON, ALBERTA, CANADA T6G 2G1. bhan@ualberta.ca mmichell@ualberta.ca yawwong@ualberta.ca